Inorg. Chem. **2007**, *46*, 4430–4445

Inorganic Chemistry
Article

Structural Characterization of Molybdenum(V) Species in Aqueous HCl Solutions

Farideh Jalilehvand,*,† Vicky Mah,† Bonnie O. Leung,† Daniel Ross,‡ Masood Parvez,† and Ricardo F. Aroca‡

Department of Chemistry, University of Calgary, Calgary, Alberta, Canada T2N 1N4, and Department of Chemistry and Biochemistry, University of Windsor, Windsor, Ontario, Canada N9B 3P4

Received October 25, 2006

Mo(V) aqua-chloro complexes in hydrochloric acid solutions have been studied by means of Mo K- and $L_{2,3}$-edge X-ray absorption and Raman spectroscopic methods. The solid compounds $(HPPh_3)_2[MoOCl_5]$ (**1**), $6[MoOCl_4(H_2O)]^-\cdot 10(pyH)^+\cdot 4Cl^-$ (**2**), and $(pyH)_2[Mo_2O_4Cl_4(trans\text{-}OH_2)_2]$ (**3**) were used for structural comparisons. The compound **2** crystallizes in the orthorhombic space group *Pmma* (no. 51) with $a = 21.398(3)$, $b = 8.057(4)$, $c = 13.330(4)$ Å, and $Z = 4$. In 0.2 M solutions of $MoCl_5$ in 7.4–9.4 M HCl the mononuclear $[MoOCl_4(OH_2)]^-$ complex dominates with the bond distances Mo═O 1.66(2) Å, Mo–Cl 2.38(2) Å, and Mo–OH_2 2.30(2) Å. Its Raman band at 994 cm^{-1} for the Mo═O symmetric stretching vibration is closer to that of **2** (988 cm^{-1}) than of **1** (969 cm^{-1}). The Mo K-edge EXAFS spectrum for 0.2 M $MoCl_5$ in 1.7 M HCl solution reveals a dinuclear $[Mo_2O_4Cl_{6-n}(OH_2)_n]^{n-4}$ ($n =$ 2, 3) complex with a double oxygen bridge and the average distances Mo═O 1.67(2) Å, Mo–(μ-O) 1.93(2) Å, Mo–Cl 2.47(3) Å, Mo–Mo 2.56(2) Å, and a short Mo–OH_2 distance of 2.15(2) Å, which implies that at least one of the aqua ligands is in equatorial position relative to the two axial Mo═O bonds. This position differs from the Mo–OH_2 configuration exclusively *trans* to the M═O groups of the isomeric (with $n = 2$) dinuclear complex in **3**. The difference in the ligand field is also reflected in their $L_{2,3}$-edge XANES spectra. For 0.2 M $MoCl_5$ solutions in intermediate HCl concentrations (3.7–6.3 M) the Raman bands at 802 cm^{-1} (Mo–O–Mo) and 738 cm^{-1} (Mo–$(\mu\text{-O})_2$–Mo) verify three coexisting classes of Mo(V) complexes: mononuclear complexes together with dinuclear mono-oxo (e.g., $[Mo_2O_3Cl_6(H_2O)_2]^{2-}$) and dioxo bridged species, even though principal component analysis (PCA) of the corresponding series of EXAFS spectra only could distinguish two major components. By fitting linear combinations of the appropriate EXAFS oscillation components, dioxo-bridged dinuclear complexes were found to dominate at HCl concentrations $\leq$ 4.5 M, a conclusion supported by the Mo $L_{2,3}$-edge XANES spectra.

Introduction

Solutions of $MoCl_5$ in hydrochloric acid display distinct color changes, from emerald green in 10 M HCl, opaque dark brown in 6 M HCl, to amber yellow in 2 M HCl.[1,2] Along with the variation in color, the magnetic properties also change. By measuring the magnetic susceptibility, Sacconi and Cini suggested that paramagnetic monomeric Mo(V) complexes with d^1 configuration are present in solutions with $c_{HCl} > 7$ M. At lower HCl concentration dimeric species form, involving electron-pairing of two Mo(V) ions. The process is completed for HCl concentrations below 2.5 M, where all Mo(V) ions are present in diamagnetic dimeric entities.[3] Since the reflectance spectrum of the green solid $(NH_4)_2[MoOCl_5]$ compound and the UV−vis spectrum of its solution in 10 M HCl were similar, Gray and Hare suggested that either $[MoOCl_5]^{2-}$ or $[MoOCl_4(H_2O)]^-$ with C_{4v} symmetry were present in 8−10 M HCl (Figure 1***a***,***b***).[4] Later, Boorman et al. concluded from an ESR study that $[MoOCl_4(OH_2)]^-$ is the monomeric Mo(V) complex formed in concentrated aqueous HCl.[5]

* To whom correspondence should be addressed. E-mail: faridehj@ucalgary.ca.
† University of Calgary.
‡ University of Windsor.

(1) El-Shamy, H. K.; El-Aggan, A. M. *J. Am. Chem. Soc.* **1953**, *75*, 1187.
(2) Jorgensen, C. K. *Acta Chem. Scand.* **1957**, 73.
(3) Sacconi, L.; Cini, R. *J. Am. Chem. Soc.* **1954**, *76*, 4239.
(4) Gray, H. B.; Hare, C. R. *Inorg. Chem.* **1962**, *1*, 363.
(5) Boorman, P. M.; Garner, C. D.; Mabbs, F. E. *J. Chem. Soc., Dalton Trans.* **1975**, 1299.

10.1021/ic062047c CCC: $37.00
Published on Web 05/03/2007

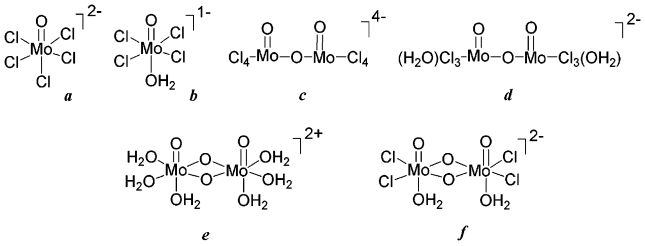

Figure 1. Previously proposed structures for dominating Mo(V) species in HCl(aq) solutions: (***a***, ***b***) HCl concentration 8−12 M [refs 2, 4−6, and 11]; (***c***, ***d***) 5−6 M HCl [refs 7 and 12]; and (***e***, ***f***) 1−2 M HCl [refs 9, 11, and 12].

Hare et al. reported that the intensity of the ESR signal, which is proportional to the amount of the molybdenyl MoO^{3+}entity in Mo(V) solutions, is drastically reduced with decreasing concentration of HCl, much faster than expected from the magnetic susceptibility data.[6] Since the magnetic susceptibility accounts for all paramagnetic species in a solution, Gray and Hare proposed an additional paramagnetic dimeric complex in 4−10 M HCl solutions with the highest concentration, ∼25−30%, at 6 M HCl. Based on electronic absorption spectra, Haight proposed a mono-oxo bridge for this paramagnetic dimer (Figure 1***c***),[7] expressing that "hydrolysis of $[MoOCl_5]^{2-}$ involves the production of a complicated sequence of dimers, the first of which is $[Cl_4OMo-O-MoOCl_4]^{4-}$".[6,7] This paramagnetic dimer converts to diamagnetic dimeric species and is negligible below 4 M HCl.[6]

Marov and co-workers concluded from ESR studies of frozen solutions with <8 M HCl that the hydrolysis of $[MoOCl_5]^{2-}$ proceeds through several steps prior to the formation of such dimers. Paramagnetic monomers appear, such as $[MoOCl_4(H_2O)]^-$, $[MoOCl_3(H_2O)_2]$, and $[MoOCl_3(H_2O)(OH)]^-$, which transform to dimers at lower HCl concentration (reaction 1), possibly with a single oxo bridge as in the $[(H_2O)Cl_3OMo-O-MoOCl_3(H_2O)]^{2-}$ complex (Figure 1***d***). They pointed out that a linear Mo−O−Mo entity would be diamagnetic.[8]

$$2\,[MoOCl_4(H_2O)]^- + H_2O \rightleftharpoons [(H_2O)Cl_3\overset{O}{\overset{\|}{Mo}}\text{-}O\text{-}\overset{O}{\overset{\|}{Mo}}Cl_3(H_2O)]^{2-} + 2H^+ + 2Cl^- \quad (1)$$

For Mo(V) in dilute HCl solutions Ardon and Pernick proposed a dioxo-bridged structure without chloro ligands, $[Mo_2O_4(H_2O)_6]^{2+}$ (Figure 1***e***), from a comparison with UV−vis spectra of the diamagnetic Mo(V) oxalato complex.[9] Himeno et al. used Raman spectroscopy to identify three types of species with Mo═O, Mo−(μ-O)−Mo and Mo−(μ-O)$_2$−Mo cores, respectively, concluding that there is an equilibrium between $[MoOCl_5]^{2-}$ and $[Mo_2O_3Cl_8]^{4-}$ in solutions with 6−7 M HCl, while this mono-oxo bridged Mo−O−Mo dimer would dominate for intermediate (3−5 M) HCl concentrations and the monomer for $c_{HCl} \geq 8$ M (Figure 1***a***,***c***). Since the Raman spectra of all Mo(V) solutions showed an Mo−Cl vibrational frequency in the 323−334 cm^{-1} region, Himeno et al. proposed structure ***f*** for Mo(V) in 1 M HCl, which differs from the previously suggested structure ***e*** (Figure 1), and that the mono-oxo and dioxo bridged species ***c*** and ***f*** would coexist in 2 M HCl solution.[10] Later, Himeno et al. reported, based on polarographic and spectroscopic studies of 0.001 M Mo(V) solutions, that 80−100% of Mo(V) is present in a $[Mo_2O_3Cl_8]^{4-}$ complex in 2−3 M HCl and ionic strength $I = 5.0$.[11]

Lincoln and Loehr combined electronic and vibrational spectroscopy to study the hydrolysis of Mo(V) in HCl. They measured Raman spectra of 0.05−0.54 M Mo(V) solutions in 10 M HCl, 0.163 M Mo(V) in 6 M HCl, and 0.05 M Mo(V) in 2 M HCl, using ^{18}O-isotopic substitution to aid assignments of Raman bands measured at 90 and 300 K, and concluded that the major Mo(V) species in 10, 5−6, and 2 M HCl solutions were represented by the structures ***a***, ***c***, and ***f*** (Figure 1), respectively.[12] The Raman band at ∼380 cm^{-1} was assigned as the symmetric Mo−O−Mo stretching for $[Mo_2O_3Cl_8]^{4-}$ (Figure 1***c***), supporting a linear Mo−O−Mo entity.[12] Consequently, the $[Mo_2O_3Cl_8]^{4-}$ complex should be diamagnetic as also other known complexes containing a linear $Mo_2O_3^{2+}$ core, a conclusion in conflict with the earlier proposal of a "paramagnetic dimer" in 6 M HCl solution.[6,7,12] However, the calculations by Blake et al. suggest that the energy difference between singlet ($S = 0$) and triplet ($S = 1$) states for a linear Mo−O−Mo entity could be very small in the absence of intermolecular constraints.[13]

Cramer et al. reported the bond distance Mo═O 1.68 Å and the distances Mo−(μ-O) 1.93 Å and Mo−Mo 2.56 Å for the double bridge in the core unit of $Mo_2O_2(\mu\text{-}O)_2^{2+}$, from an Mo K-edge EXAFS study on Mo(V) in 3 M HCl, with no further information about the identity of the terminal ligands and/or their distances from the molybdenum ion.[14] Yokoi and co-workers measured Mo K-edge EXAFS spectra for a series of Mo(V) solutions with different HCl concentration in an attempt to determine the structure of the $[Mo_2O_3Cl_8]^{4-}$ complex. They suggested that the Mo−O−Mo angle in this complex is about 104−111°.[15] However, the interpretation of the EXAFS spectra was performed by analyzing the position of the peaks in the Fourier-transforms, which is not a reliable procedure.

Despite the numerous studies performed on this apparently simple system and the known crystal structures of $[MoOCl_5]^{2-}$ and $[Mo_2O_4Cl_4(H_2O)_2]^{2-}$ (Figure 1***a***, ***e***), some uncertainty still remains about the structures of the Mo(V) species in HCl solution. The current structural investigation of $MoCl_5$ solutions in different HCl concentrations systematically combines Mo K- and $L_{2,3}$- edge X-ray absorption and Raman

(6) Hare, C. R.; Bernal, I.; Gray, H. B. *Inorg. Chem.* **1962**, *1*, 831.
(7) Haight, G. P. *J. Inorg. Nucl. Chem.* **1962**, *24*, 663.
(8) Marov, I. N.; Dubrov, Y. U.; Evtikova, G. A.; Belyaeva, V. K.; Ermakov, A. N.; Korovaikov, P. A. *Russ. J. Inorg. Chem.* **1970**, *15*, 1148.
(9) Ardon, M.; Pernick, A. *Inorg. Chem.* **1973**, *12*, 2484.
(10) Himeno, S.; Hasegawa, M. *Inorg. Chim. Acta* **1984**, *83*, L17.
(11) Himeno, S.; Saito, A.; Hasegawa, M. *Inorg. Chim. Acta* **1984**, *88*, 93.
(12) Lincoln, S. E.; Loehr, T. M. *Inorg. Chem.* **1990**, *29*, 1907.
(13) Blake, A. B.; Cotton, F. A.; Wood, J. S. *J. Am. Chem. Soc.* **1964**, *86*, 3024.
(14) Cramer. S. P.; Eidem, P. K.; Paffet, M. T.; Winkler, J. R.; Dori, Z.; Gray, H. B. *J. Am. Chem. Soc.* **1983**, *105*, 799.
(15) Yokoi, K.; Matsubayahi, N.; Miyanaga, T.; Watanabe, I.; Ikeda, S.; Murata, K. *Polyhedron* **1989**, *8*, 45.

spectroscopy with information from crystal structures and theoretical calculations, to further clarify the nature of the species in such solutions.

Experimental Procedures

Sample Preparation. $MoCl_5$ powder (99.9%), supplied by Sigma-Aldrich, was dissolved in aqueous HCl prepared by diluting concentrated hydrochloric acid (36.86%; 11.9 M from EM Science). The measured density varied between 1.15 g mL^{-1} for 9.4 M HCl to 1.03 g mL^{-1} for 1.7 M HCl and was compared with tabulated values to obtain the concentration of the diluted HCl acid within ±3%.[16] Each HCl solution was also diluted to 0.1 M and titrated potentiometrically with 0.105 N NaOH (Sigma-Aldrich). Solutions of $MoCl_5$ (~0.2 M) in HCl of different concentration (1.7−9.4 M) for EXAFS measurements were prepared under argon atmosphere by dropwise addition of the corresponding cold acid to a chilled flask containing $MoCl_5$ powder, 3 days before transport to the synchrotron facilities.

Separate sets of solutions were prepared for the Raman measurements, keeping the same timeline as for the EXAFS study. Oxidation of Mo(V) to Mo(VI) was monitored by measuring Raman spectra of the solutions at different time intervals (Figure S-2). Crystals of **1** and **3** were obtained by procedures described previously in the literature[17,18] and identified by determining the unit cell dimensions by XRD. Compound **2** was prepared as green crystals according to a method originally reported for synthesis of solid $(pyH)_2[MoCl_5]$.[19] By solving the crystal structure, we could show that **2** contains a $(pyH)[MoOCl_4(H_2O)]$ complex. Attempts for synthesis of $Cs_4[Mo_2O_3Cl_8]$ according to the proposed method by Colton and Rose failed.[20] Cotton et al. also found this synthesis difficult to reproduce.[21]

Compound 2. Hydrazine hydrate (31.5 mmol, 1.53 mL) was added dropwise to HCl (11.9 M, 90 mL) while the mixture was being stirred. The milky white solution was added to a flask containing $Na_2MoO_4{\cdot}2H_2O$ (17.1 mmol, 4.13 g) under Ar, and the mixture was stirred in a water bath heated to 80 °C for 3 h. The bright green solution was slowly cooled to room temperature and then placed into a freezer overnight. The solution was filtered cold to remove precipitated NaCl. Pyridine (4.5 mL) was added dropwise to the green filtrate at room temperature. When the solution was cooling to 0 °C, green needle-shape crystals were obtained, which were dried under vacuum; yield = 5.57 g (92.7%). Exp. %C 23.47, %H 2.23, %N 5.07. Calc for $6[MoOCl_4(OH_2)]^-{\cdot}10(pyH)^+{\cdot}4Cl^-$ ($C_{12.5}H_{18}Cl_7Mo_{1.5}N_{2.5}O_3$): %C 23.3, %H 2.83, %N 5.44.

Crystal Structure of 2. Intensity data were collected from a green prismatic crystal mounted on a glass fiber, by means of a Nonius Kappa CCD diffractometer with graphite monochromated Mo-K_α radiation, using ω and φ scans up to $\theta = 27.5°$.[22] A primitive orthorhombic unit cell was found with cell constants refined for 5135 reflections in the range $1.9 < \theta < 27.5°$; details of crystal data and structure refinement are provided in Table 1.[23] No decay correction was needed for the intensity data, which were corrected for Lorentz and polarization effects and for absorption using the multiscan method.[23] The structure was solved by direct methods and expanded using Fourier techniques in SHELXL97.[24−26] All non-hydrogen atom were refined allowing anisotropic displacements. Disordered positions were found for the Cl3 atom and a C_5H_6N ring (Figure 2). Hydrogen atoms were introduced (except for the water molecules) without refinement at geometrically idealized positions. Atomic coordinates and selected bond distances and angles are presented in Tables S-1 and S-2.

Table 1. Crystallographic Data and Structure Refinement for $6[MoOCl_4(H_2O)]^-{\cdot}10(pyH)^+{\cdot}4Cl^-$ (**2**)

empirical formula	$C_{12.5}H_{18}Cl_7Mo_{1.5}N_{2.5}O_3$
formula weight	643.35
temperature (T)	173(2) K
wavelength (λ)	0.71073 Å
crystal system	orthorhombic
space group	*Pmma* (no. 51)
unit cell dimensions	a = 21.398(3) Å
	b = 8.057(4) Å
	c = 13.330(4) Å
volume	2298.1(14) $Å^3$
Z	4
density (calculated)	1.859 g/cm^{-3}
absorption coefficient (μ)	1.662 mm^{-1}
no. of collected reflns	5135
no. of unique reflns (R_{int})	2888 (0.031)
no. of obsd reflns ($I > 2\sigma I$)	2179
no. of parameters	160
R (F)[a] (obsd reflns)	0.036
R_w (F^2)[a] (all reflns)	0.098
GOF	0.99

[a] $R(F) = \Sigma||F_o| - |F_c||/\Sigma|F_o|$. $R_w(F^2) = \{\Sigma[w(F_o^2 - F_c^2)^2]/\Sigma[w(F_o^2)^2]\}^{1/2}$.

Electronic Absorption Spectroscopy. UV−vis spectra of 0.2 M $MoCl_5$ solutions in 1.7−9.4 M HCl (Figure S-1) were measured in quartz cells with path length 0.1 cm using a Varian CARY-219 spectrophotometer. Aqueous HCl solutions with similar concentra-

(16) Lide, D. R. *CRC: Handbook of Chemistry and Physics*, 87th ed.; 2006; p 8−53.
(17) Junk, P. C.; Atwood, J. L. *J. Coord. Chem.* **1999**, *46*, 505.
(18) Jezowska-Trzebiatowska, B.; Rudolf, M. F.; Natkaniec, L.; Sabat, H. *Inorg. Chem.* **1974**, *13*, 617.
(19) Hanson, G. R.; Brunette, A. A.; McDonell, A. C.; Murray, K. S.; Wedd, A. G. *J. Am. Chem. Soc.* **1981**, *103*, 1953.
(20) Colton, R.; Rose, G. G. *Aust. J. Chem.* **1968**, *21*, 883.
(21) Cotton, F. A.; Hunter, D. L.; Licard, L.; Weiss, R. *J. Coord. Chem.* **1974**, *3*, 259.
(22) Hooft, R. *COLLECT*: *Users Manual*; Nonius B.V., Delft: The Netherlands, 1998.
(23) Otwinowski, Z.; Minor, W. *Processing of X-ray Diffraction Data Collected in Oscillation Mode, Methods in Enzymology;* Carter, C. W., Jr., Sweet, R. M., Eds.; Academic Press: 1997; Vol. 276, Macromolecular Crystallography, Part A, pp 307−326.
(24) Altomare, A.; Cascarano, M.; Giacovazzo, C.; Guagliardi, A. *J. Appl. Cryst.* **1993**, *26*, 343.
(25) Beurskens, P. T.; Admiraal, G.; Beurskens, G.; Bosman, W. P.; de Gelder, R.; Israel, R.; Smits, J. M. M. *The DIRDIF-94 program system*; Technical Report of the Crystallography Laboratory; University of Nijmegen: The Netherlands, 1994.
(26) Sheldrick, G. M. *SHELXL97- A Program for Refinement of Crystal Structures*; University of Göttingen: Germany, 1997.
(27) Johnson, C. K. *ORTEPII*; Report ORNL-5138; Oak Ridge National Laboratory: Oak Ridge, TN, U.S.A., 1976.
(28) Frisch, M. J.; Trucks, G. W.; Schlegel, H. B.; Scuseria, G. E.; Robb, M. A.; Cheeseman, J. R.; Montgomery, J. A., Jr.; Vreven, T.; Kudin, K. N.; Burant, J. C.; Millam, J. M.; Iyengar, S. S.; Tomasi, J.; Barone, V.; Mennucci, B.; Cossi, M.; Scalmani, G.; Rega, N.; Petersson, G. A.; Nakatsuji, H.; Hada, M.; Ehara, M.; Toyota, K.; Fukuda, R.; Hasegawa, J.; Ishida, M.; Nakajima, T.; Honda, Y.; Kitao, O.; Nakai, H.; Klene, M.; Li, X.; Knox, J. E.; Hratchian, H. P.; Cross, J. B.; Bakken, V.; Adamo, C.; Jaramillo, J.; Gomperts, R.; Stratmann, R. E.; Yazyev, O.; Austin, A. J.; Cammi, R.; Pomelli, C.; Ochterski, J. W.; Ayala, P. Y.; Morokuma, K.; Voth, G. A.; Salvador, P.; Dannenberg, J. J.; Zakrzewski, V. G.; Dapprich, S.; Daniels, A. D.; Strain, M. C.; Farkas, O.; Malick, D. K.; Rabuck, A. D.; Raghavachari, K.; Foresman, J. B.; Ortiz, J. V.; Cui, Q.; Baboul, A. G.; Clifford, S.; Cioslowski, J.; Stefanov, B. B.; Liu, G.; Liashenko, A.; Piskorz, P.; Komaromi, I.; Martin, R. L.; Fox, D. J.; Keith, T.; Al-Laham, M. A.; Peng, C. Y.; Nanayakkara, A.; Challacombe, M.; Gill, P. M. W.; Johnson, B.; Chen, W.; Wong, M. W.; Gonzalez, C.; Pople, J. A. *Gaussian 03, Revision B.03*; Gaussian Inc.: Pittsburgh, PA, 2003.

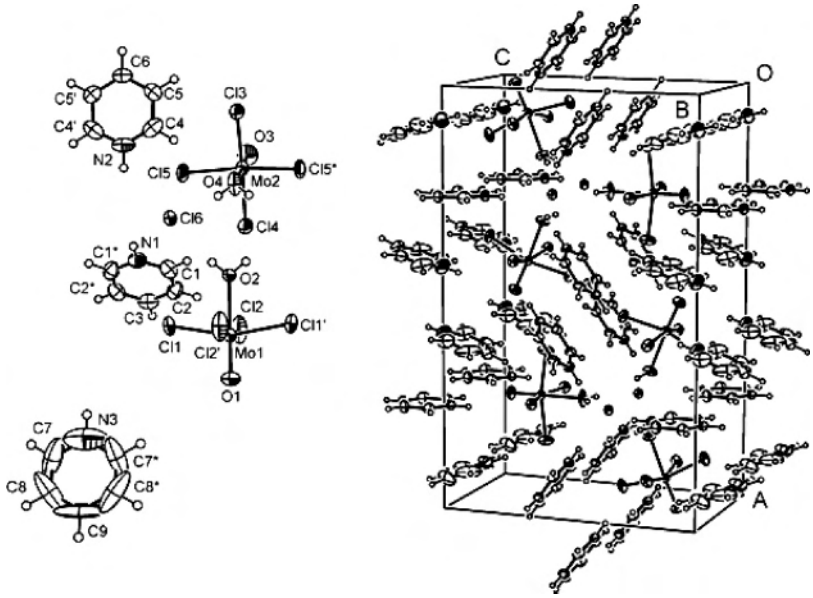

Figure 2. ORTEPII[27] plots for $6[MoOCl_4(H_2O)]^-\cdot 10(pyH)^+\cdot 4Cl^-$ (**2**).

tions as the Mo(V) samples were used as blank. For further description and discussion, see Appendix 2 in the Supporting Information.

Raman Spectroscopy. Raman spectra were collected of the solutions within glass vials on a RM2000 Renishaw Raman Microscope using 514 nm laser excitation, about 10 mW at the sample. The spectra were calibrated versus the 520 cm^{-1} peak of a Si mirror. For $MoCl_5$ solutions in 1.7−2.7 and 5.4−9.4 M HCl, between 10 and 25 scans were averaged, while for 3.7, 4.5, and 4.9 M HCl solutions a total of 85, 150, and 45 scans were collected, respectively. The Raman spectra of the 4.5−4.9 M and 7.4−9.4 M HCl solutions were measured with 1.8 cm^{-1} resolution and subjected to mild smoothing (25% Fourier-transform) in the GRAMS AI program, while the resolution for other solutions was 5 cm^{-1}. The intensities of the Raman bands for solutions were scaled arbitrarily, since no internal calibration (e.g., with perchlorate) was used during the measurements. The Raman spectra of **1**−**3** as well as for the oxidized solutions (Figure S-2, left) were measured with 2 cm^{-1} resolution using a Bruker RAMII FT-Raman with 1064 nm laser excitation. Background subtraction was performed using polynomials in Bruker's OPUS program.

Theoretical Calculations of Raman Spectra. Raman spectra were simulated theoretically using the GAUSSIAN 03 suite of programs.[28] Density functional theory (DFT) calculations were carried out using the hybrid functional B3LYP, comprised of Becke's 3-parameter exchange functional[29] and the correlation function due to Lee, Yang, and Parr.[30] For molybdenum the Lanl2dz basis set with the Los Alamos ECP was used.[31] The optimization was performed without symmetry constraints, employing tight convergence criteria. The resulting Raman frequencies were not scaled (Figure S-4a,b).

XAS Data Collection. The Mo K-edge X-ray absorption spectra were recorded in transmission mode at beamline 10-B of the Photon Factory of the High Energy Accelerator Research Organization (Tsukuba, Japan) under dedicated conditions (2.5 GeV with critical energy of 4 keV, 300−400 mA). Monochromatization was achieved by means of a fully tuned Si(311) channel-cut monochromator crystal for which the ratio of higher order harmonics is very low (less than 2×10^{-5} at 21.8 keV). The first ion chamber was filled with argon and the second one with krypton. The energy scale was externally calibrated before and after each sample by assigning the first inflection point of a molybdenum foil to 20 003.9 eV. Three scans were collected for each sample at room temperature with the solutions held in 5 mm Teflon cells with 4 μm polypropylene film as window material. The solid samples were finely ground and mixed with boron nitride.

Mo L-edge X-ray absorption near-edge structure (XANES) spectra were collected at the 54-pole wiggler beamline 6-2 at the Stanford Synchrotron Radiation Laboratory (SSRL) with the storage ring operating at 3.0 GeV and 80−100 mA. Harmonics from the fully tuned Si(111) double crystal monochromator were rejected using a Ni-coated mirror. The samples were kept under helium atmosphere with the solutions in 1 mm Teflon cells with 4 μm polypropylene film windows and with a fine powder of the solids dusted on Mylar tape. Two energy scans were performed using nitrogen in a fluorescence (Lytle) detector, with helium in the monitor ion chamber I_0. The energy scale of the Mo L_2, L_3-edge spectra was externally calibrated by assigning the first peak maximum in the S K-edge XANES spectrum of $Na_2S_2O_3\cdot 5H_2O$ to 2472.02 eV. The scans were averaged and background corrected, and each edge step was normalized at the Mo L_3 and L_2 absorption edges, at 2550 and 2655 eV, respectively. For Mo(V) in 4.9 M HCl, the detector became saturated at the L_2-edge.

EXAFS Data Analysis. The experimental Mo K-edge EXAFS oscillations (Figure 3) were extracted according to the previously described procedure,[32] by subtracting a nine segment cubic spline using the WinXAS 3.1 package.[33] The energy scale was converted to k-space, where $k = (8\pi^2 m_e/h^2)(E-E_0)$, using the threshold energy, E_0, shown in Table S-6. The EXAFS oscillations of **1**−**3** and of the $MoCl_5$ solutions in 1.7−2.7 and 7.4−9.4 M HCl were analyzed to obtain structural information of their single dominating Mo complex. The EXAFS model functions, $\chi(k)$, were constructed with structural information from the crystal structures of **1**−**3** (Figure 4), using the FEFF 8.1 program to obtain ab initio calculated

(29) Becke, A. D. *J. Chem. Phys.* **1993**, *98*, 5648.
(30) Lee, C.; Yang, W.; Parr, R. G. *Phys. Rev. B* **1988**, *37*, 785.
(31) Hay, P. J.; Wadt, W. R. *J. Chem. Phys.* **1985**, *82*, 270.
(32) Jalilehvand, F.; Leung, B. O.; Izadifard, M.; Damian, E. *Inorg. Chem.* **2006**, *45*, 66.
(33) Ressler, T. *J. Synchrotron Radiat.* **1998**, *5*, 118.

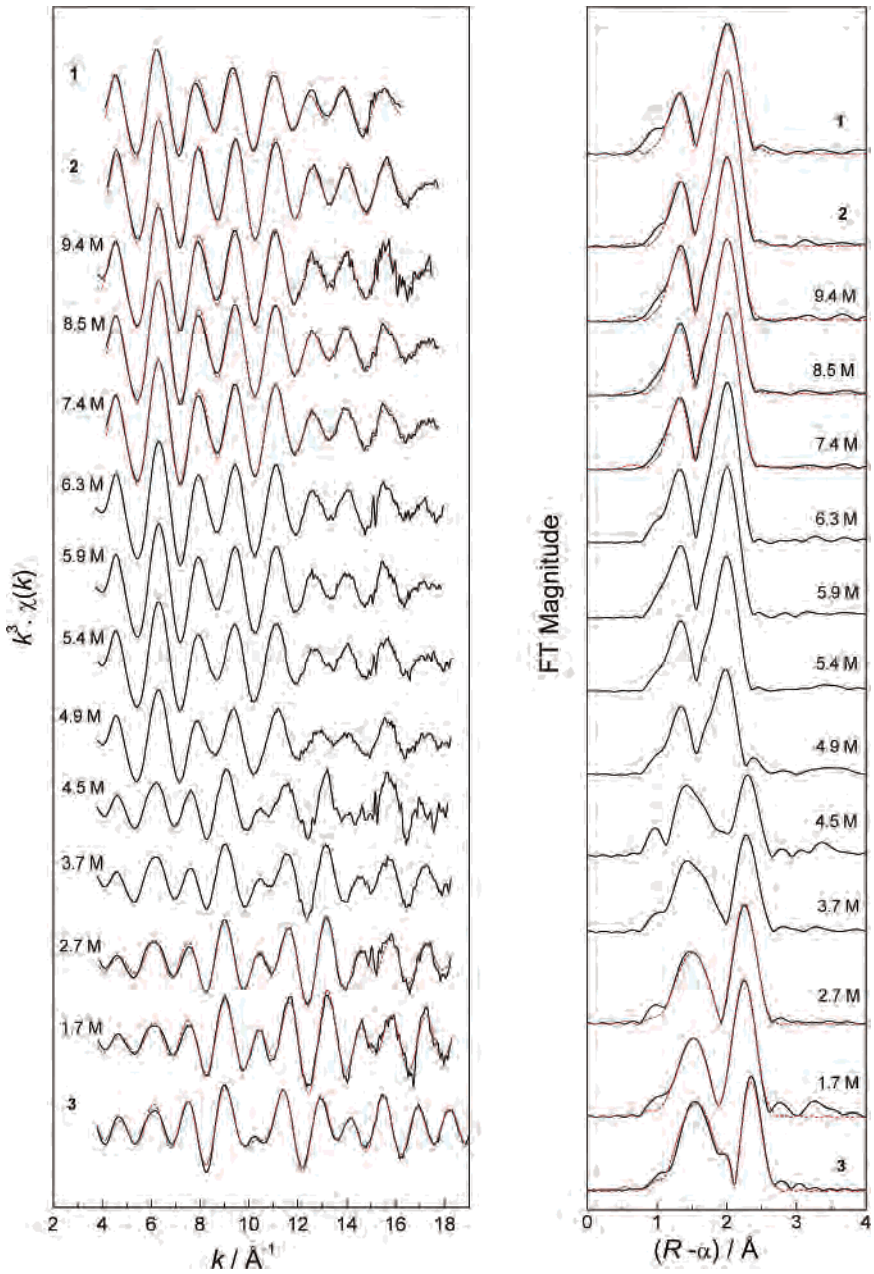

Figure 3. (left) k^3-weighted Mo K-edge EXAFS oscillations with (right) Fourier transforms (without phase shift correction) for **1**−**3** and 0.2 M $MoCl_5$ solutions in 1.7−9.4 M HCl. The fitted $k^3 \cdot \chi(k)$ model functions and their FT transforms are shown as red dashed lines (- - -).

amplitude $f_{\mathrm{eff}}(k)_i$, phase shift $\phi_{ij}(k)$, and mean free path $\lambda(k)$ functions.[34,35]

$$\chi(k) = \sum_i \frac{N_i \cdot S_0^2(k)}{k \cdot R_i^2} |f_{\mathrm{eff}}(k)|_i \cdot \exp(-2k^2\sigma_i^2) \cdot \exp[-2R_i/\Lambda(k)] \cdot \sin[2kR_i + \phi_{ij}(k)] \quad (2)$$

The structural parameters were refined by least-squares methods, fitting the k^3-weighted theoretical model function $\chi(k)$ to the experimental unfiltered EXAFS oscillations over the k range 3.8−18.2 Å $^{-1}$ (16.2 Å^{-1} for **1**), by keeping the coordination number (N_i) constant and allowing distance (R), Debye−Waller parameter (σ), amplitude reduction factor (S_0^2), and ΔE_0 (linked parameter for all scattering paths) to float. The ΔE_0 values fluctuated between 12.6 and 14.4 eV for **1**, **2**, and the solutions and 15.3 eV for **3**. The fitting results for **1**−**3** and for the $MoCl_5$ solutions in 1.7−2.7 M and 7.4−9.4 M HCl are shown in Figure 3 and Table 2. The accuracy of the bond distances and their Debye−Waller parameters are within ±0.02 Å and ±0.0005 Å,^{2} respectively.

Principal component analysis (PCA), introduced in the EXAFSPAK program package,[36] was applied on the raw k^3-weighted experimental EXAFS spectra, showing two major PCA components. TARGET in the EXAFSPAK program package displayed that the two components were similar to the EXAFS oscillations of the $MoCl_5$ solutions in 1.7 M HCl and in 7.4 M HCl (or **2**) (see Figures

(34) Teo, B. K. *EXAFS- Principles and Data Analysis*; Springer-Verlag: Berlin, 1986; Chapter 5, pp 84−89.

(35) (a) Mustre de Leon, J.; Rehr, J. J.; Zabinsky, S. I.; Albers, R. C. *Phys. Rev. B* **1991**, *44*, 4146. (b) Zabinsky, S. I.; Rehr, J. J.; Ankudinov, A.; Albers, R. C.; Eller, M. J. *J. Phys. Rev. B* **1995**, *52*, 2995. (c) Ankudinov, A. L.; Rehr, J. J. *J. Phys. Rev. B* **1997**, *56*, R1712.

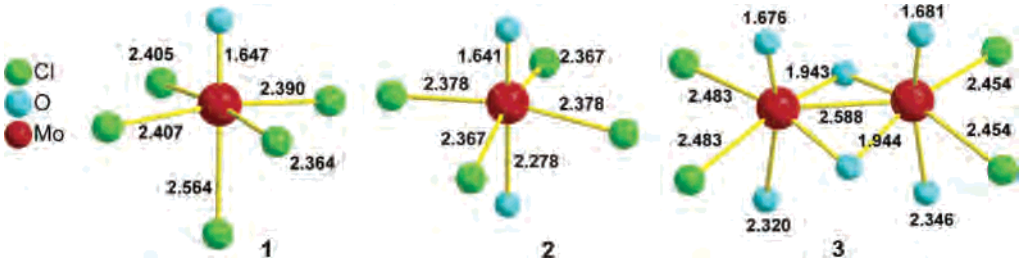

Figure 4. Structural models used for FEFF calculations were obtained from the crystal structures **1**−**3** (refs 17 and 37 and **2** in this study).

Table 2. Results of Least-Squares $k^3 \cdot \chi(k)$ Model Fitting to the EXAFS Oscillations for the Solid Compounds **1**−**3** and 0.2 M $MoCl_5$ Solutions in HCl of Different Concentrations[a]

	Mo═O			Mo-Cl			additional contributions				
Mo(V) species	C.N	R (Å)	σ^2 (Å^2)	C.N	R (Å)	σ^2 (Å^2)		C.N	R (Å)	σ^2 (Å^2)	S_0^2
1	1	1.66	0.0013 *f*	4	2.40	0.0038	Mo-Cl	1	2.55	0.0065	0.89
2	1	1.66	0.0013 *f*	4	2.39	0.0038	Mo−OH_2	1	2.27	0.0030 *f*	1.00
9.4 M HCl	1	1.66	0.0013 *f*	4	2.38	0.0042	Mo−OH_2	1	2.30	0.0030 *f*	1.06
7.4−8.5 M HCl	1	1.66	0.0012	4	2.38	0.0045	Mo−OH_2	1	2.30	0.0030 *f*	1.05
3	1	1.67	0.0013 *f*	2	2.43	0.0062	μ-Mo−O	2	1.94	0.0022	1.04
							Mo−OH_2	1	2.31	0.0032	
							Mo−Mo	1	2.61	0.0022	
1.7 M HCl	1	1.67	0.0013 *f*	2	2.47	0.0140 [b]	μ-Mo−O	2	1.93	0.0022	0.99
(model *1*)							Mo−OH_2	1	2.15	0.0038	
							Mo−Mo	1	2.56	0.0019	
(model *2*)[c]	1	1.67	0.0013 *f*	1.5	2.48	0.0125 [b]	μ-Mo−O	2	1.93	0.0022	1.01
							Mo−OH_2	1.5	2.15	0.0056	
							Mo−Mo	1	2.56	0.0020	
2.7 M HCl	1	1.68	0.0013 *f*	2	2.48	0.0155 [b]	μ-Mo−O	2	1.94	0.0034	1.07
							Mo−OH_2	1	2.18	0.0042	
							Mo−Mo	1	2.56	0.0026	

[a] *f* = fix; coordination numbers were fixed. [b] The estimated error in σ^2 is ±0.0010 Å.^{2} [c] $[Mo_2O_4Cl_3(H_2O)_3]^-$ model; fitting not shown in Figure 3. Coordination no. = 1.5 is an average for the two Mo centers.

S-8 and S-9 in Appendix 6, Supporting Information). The DATFIT program in the EXAFSPAK package was then used to fit linear combinations of the EXAFS spectra of $MoCl_5$ solutions in 1.7 and 7.4 M HCl (or **2**) to the raw experimental EXAFS spectra of the $MoCl_5$ solutions with HCl concentrations of 3.7−6.3 M to estimate their percentage of the dioxo-bridged dinuclear Mo(V) species (Figure S-12 and Table S-7). For a detailed discussion, see Appendix 6 in Supporting Information.

Theoretical Calculations of Molecular Orbitals. The electronic structure of the mononuclear $[MoOCl_4(H_2O)]^-$ complex in **2**, different ligand configurations for the dinuclear $[Mo_2O_4Cl_4(H_2O)_2]^{2-}$ species, and the $[Mo_2O_4Cl_3(H_2O)_3]^-$ complex were investigated with theoretical calculations. The *xyz* coordinates were obtained from the crystal structures of **2** and **3**[37] and from the Mo K-edge EXAFS refinement and applied on the same geometry as in crystal **3** (Figure S-16 and Table S-10*a*−*e*).

Single-point DFT calculations were performed with the Amsterdam Density Functional (ADF) program using the triple-ζ small frozen core basis set with polarization functions for H, Cl, and O.[38−40] The scalar relativistic zero-order regular approximation (ZORA) method, implemented in the ADF code, was used for Mo and calculated with the all-electron standard basis sets: ZORA-TZP. The density functional exchange was described by the Slater-type local density approximation (LDA),[41,42] and the Becke GGA functional.[43] Nonlocal gradient corrections were used for exchange[43] and for correlation effects.[44] Spin-unrestricted calculations were carried out for the mononuclear complex, while the dinuclear complexes were analyzed with spin-restricted computations.

Results and Discussion

Raman Spectroscopy. Raman spectra of **1**−**3** and the Mo(V) solutions in 1.7−9.4 M HCl are shown in Figure 5, with corresponding band assignments presented in Table 3.[12] Raman spectra recorded of the solutions at different time intervals are useful to monitor possible oxidation of Mo(V) to Mo(VI), as shown in Figure S-2. Partial oxidation of Mo(V) to Mo(VI) gives rise to a new peak at 960 cm^{-1} for all solutions, which is close to the Mo═O stretching band for crystalline $[Mo^{VI}O_2Cl_2(H_2O)_2]^-$ at 951 cm^{-1}.[45]

(36) George, G. N.; Pickering, I. J. *EXAFSPAK: A Suite of Computer Programs for Analysis of X-ray Absorption Spectra*; SSRL: Stanford, CA, 1995.
(37) (a) Glowiak, T.; Sabat, M. *J. Cryst. Mol. Struct.* **1975**, *5*, 247. (b) Glowiak, T.; Rudolf, M. F.; Sabat, M.; Jezowska-Trzebiatowska, B. *J. Less Common Met.* **1977**, *54*, 35.
(38) Fonseca Guerra, C.; Visser, O.; Snijders, J. G.; te Velde, G.; Baerends, E. J. *Methods and Techniques in Computational Chemistry METECC-95*; Clementi, E., Corongiu, C., Eds.; STEF: Cagliari, Italy, 1995; p 305.
(39) te Velde, G.; Bickelhaupt, F. M.; Baerends, E. J.; Fonseca, Guerra, C.; van Gisbergen, S. J. A.; Snijders, J. G.; Ziegler, T. *J. Comput. Chem.* **2001**, *22*, 931.
(40) Baerends, E. J.; te Velde, B.; Rauk, A.; Ziegler, T. *ADF 2004.01; Scientific Computing and Modelling, Theoretical Chemistry*; Vrije Universiteit: Amsterdam, The Netherlands, 2004.
(41) Hohenberg, P.; Kohn, W. *Phys. Rev.* **1964**, *136*, B864.
(42) Kohn, W.; Sham, L. T. *Phys. Rev.* **1965**, *140*, A1133.
(43) Becke, A. D. *Phys. Rev. A: Gen. Phys.* **1988**, *38*, 3098.
(44) Perdew, J. P. *Phys. Rev. B* **1986**, *33*, 8822.
(45) Taylor, M. J.; Rickard, C. E. F.; Kloo, L. A. *J. Chem. Soc., Dalton Trans.* **1998**, 3195.

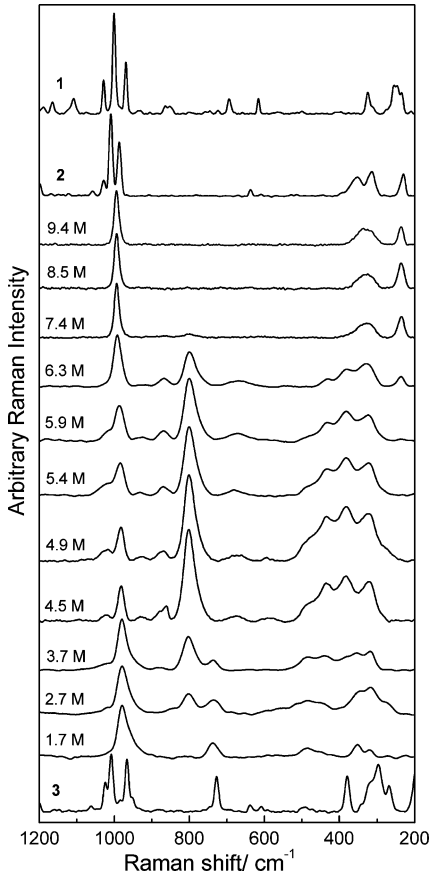

Figure 5. Baseline corrected Raman spectra (arbitrary intensity scale) of the solid compounds **1**−**3** and 0.2 M $MoCl_5$ solutions in 1.7−9.4 M HCl.

The Raman spectra for the $MoCl_5$ solutions in 7.4−9.4 M HCl are very similar. The Mo═O stretching mode at 994 cm^{-1} with a shoulder at 981−983 cm^{-1} indicates that the same Mo(V) species are present in these solutions (see Figure S-9). Previously, a similar band at 995 cm^{-1} in the Raman spectrum of Mo(V) in 10 M HCl was assigned to $[MoOCl_5]^{2-}$.[12]

To assist the structural characterization of the Mo(V) complexes in solution, Raman spectra were measured of the mononuclear Mo(V) crystalline solids $(HPPh_3)_2[MoOCl_5]$ (**1**) and $6[MoOCl_4(H_2O)]^-\cdot 10(pyH)^+\cdot 4Cl^-$ (**2**). The Raman band for Mo═O stretching appears at higher frequency for **2** (988 cm^{-1}) than for **1** (969 cm^{-1}); cf. Figure 5. A similar trend was found for the theoretically calculated Raman spectra for the $[MoOCl_5]^{2-}$ and $[MoOCl_4(H_2O)]^-$ species, with the Mo═O stretching frequencies 967 and 1013 cm^{-1}, respectively (Figure S-4a and Table S-5a,b). The Mo═O symmetric stretching frequency (A_1) is 975 cm^{-1} for $(NH_4)_2[MoOCl_5]$.[46] The ligand *trans* to the Mo═O group is often weakly bonded to the Mo^V ion,[47] and the decrease in υ(Mo═O) for **1** relative to **2** shows that the chloro ligand weakens the Mo═O bond more than the aqua ligand in *trans* position. The frequency of the υ(Mo═O) band in the Raman spectra of the $MoCl_5$ solutions in 7.4−9.4 M HCl (994 cm^{-1}), in comparison with those of **1** (969 cm^{-1}) and **2** (988 cm^{-1}) as well as the trend in the theoretically calculated Raman bands for $[MoOCl_5]^{2-}$ (967 cm^{-1}) and $[MoOCl_4(H_2O)]^-$ (1013 cm^{-1}), indicates that the mononuclear Mo(V) species in these solutions is $[MoOCl_4(H_2O)]^-$, rather than the previously proposed $[MoOCl_5]^{2-}$ (cf. reaction 3).[1,2,12] The EXAFS results also support this conclusion.

$$MoCl_5 + 2H_3O^+ \leftrightarrow [MoOCl_4(H_2O)]^- + 4H^+ + Cl^- \quad (3)$$

For $MoCl_5$ solutions in HCl with concentrations from 2.7 to 6.3 M the intense Raman band at 800−803 cm^{-1} and two weaker bands at 435−444 cm^{-1} and 380−387 cm^{-1} in Figure 5 have been assigned as the asymmetric stretching, bending, and symmetric stretching modes, respectively, of the Mo−O−Mo bridge in a linear or near-linear mono-oxo bridged dinuclear species, such as the $[Mo_2O_3Cl_8]^{4-}$ complex.[12] The Raman band at ∼800 cm^{-1} has its highest relative intensity between 4.5 and 5.9 M HCl.

According to the UV−vis spectra, the solution of 0.2 M $MoCl_5$ in 4.9 M HCl with highest $\Delta\epsilon$ at 726 nm contains the highest concentration of the mono-oxo bridged Mo(V) species (see Appendix 2 in Supporting Information). In the Raman spectrum of 0.2 M $MoCl_5$ in 6.3 M HCl, the main Mo═O stretching band appears at 993 cm^{-1} with a shoulder at 981 cm^{-1}, as also observed in the spectra of 7.4−9.4 M HCl solutions. This shoulder grows and becomes the major Mo═O band in the Raman spectra of $MoCl_5$ solutions at lower HCl concentrations, appearing at 986 cm^{-1} for 5.9 M HCl and at 980−983 cm^{-1} for 1.7−5.4 M HCl (see Figure S-3). The Raman spectra of the $MoCl_5$ solutions in 1.7−3.7 M HCl show the Mo═O stretching band at 980 cm^{-1} with a shoulder in the 956−962 cm^{-1} region (see Figure S-3) and also a band at 735−737 cm^{-1}, cf. Figure 5. Previously, a band observed at 741 cm^{-1} for Mo(V) in 2 M HCl was assigned as the Mo−O−Mo stretching in the dioxo-bridged dinuclear complex $[Mo_2O_4Cl_4(H_2O)_2]^{2-}$.[12] For $Na_2[Mo_2O_2(\mu\text{-}O)_2(cys)_2]\cdot 5H_2O$, a band at 738 cm^{-1} was assigned as the breathing mode of the $Mo_2(\mu\text{-}O)_2$ ring.[48] For the crystalline dinuclear Mo(V) complex **3**, the Mo═O and $Mo_2(\mu\text{-}O)_2$ vibrational modes are found at 966 and 727 cm^{-1}, respectively (see Table S-4). Hence, the Raman spectra of Mo(V) in 1.7 M HCl and the solid compound **3** indicate a structural difference.

As Lincoln and Loehr proposed,[12] three different types of Mo(V) complexes should be present in various HCl concentrations: mononuclear complexes and species with mono-oxo (Mo_2O_3) and dioxo (Mo_2O_4) bridges. For the entire series of Mo(V) HCl solutions, the Mo−Cl bands between 314 and 330 cm^{-1} confirm chloro ligation.[12] The above observations indicate that mononuclear species with a Mo═O stretching band at ∼994 cm^{-1} dominate in HCl concentrations between 6.3 M and 9.4 M. In more dilute HCl solutions (≤5.9 M), dinuclear Mo(V) complexes dominate, for which the Mo═O stretching band shifts to lower wavenumbers (∼980−986

(46) Cotton, F. A.; Wing, R. M. *Inorg. Chem.* **1965**, *4*, 867.
(47) Cotton, F. A.; Wilkinson, G.; Murillor, C. A.; Bochmann, M. *Advanced Inorganic Chemistry*; John Wiley & Sons: 1980; pp 716, 870.
(48) Ueyama, N.; Nakata, M.; Araki, T.; Nakamura, A.; Yamashita, S.; Yamashita, T. *Inorg. Chem.* **1981**, *20*, 1934.

Table 3. Selected Raman Frequencies (cm^{-1}) for 0.2 M $MoCl_5$ Solutions in Different HCl Concentrations[a]

9.4 M	8.5 M	7.4 M	6.3 M	5.9 M	5.4 M	4.9 M	4.5 M	3.7 M	2.7 M	1.7 M	assignment
				1019 sh,	1016 sh,	1031 sh,	1022 sh,	1024 sh,	1019 sh,		υ (Mo═O)[b]
994 s,	994 s,	994 s,	993 s,	986 m	983 m	1015 sh,	982 m	981 s,	980 s,	980 s,	
983 sh	981 sh	982 sh	981 sh			991 sh,		962 sh	956 sh	960 sh	
						981 m					
			868 w	869 w	869 w	871 w	861 w				2δ (Mo−O−Mo)[b]
		800 m	801 s	801 s	802 s	802 s	803 s	802 m	802 w		υ_{as} (Mo−O−Mo)[b]
								737 w	735 w	737 w	υ (Mo−O_2−Mo)[c]
			435 w	435 m	436 m	435 s	437 s	437 w	444 sh		δ (Mo−O−Mo)[b]
			380 w	382 m	381 m	383 s	382 s	387 sh			υ_s (Mo−O−Mo)[b]
331 br	329 br	328 br	327 m	323 m	323 m	322 s	321 s	316 w	314 w	319 w	υ (Mo−Cl)[b]
237 m	237 m	237 m	237 w	238 w							δ (Mo═O)[c]
										224	

[a] Laser wavelength 514 nm; s = strong, m = medium, w = weak, sh = shoulder, br = broad. [b] Reference 12. [c] References 10 and 49.

cm^{-1}) and additional bands emerge at ∼800 and 737 cm^{-1} for mono-oxo (in 2.7−6.3 M HCl) and dioxo (in 1.7−3.7 M HCl) bridged species, respectively. Mo K-edge EXAFS spectroscopy was used to further investigate the structure of those Mo(V) species.

Calculated Raman spectra for **2**, $[Mo_2O_3Cl_6(H_2O)_2]^{2-}$, with a nearly linear (164 °) Mo−O−Mo entity, and for **3** show a similar shift of the Mo═O stretching, from 1013 to 1003 to 982 cm^{-1}, respectively (see Figure S-4a,b and Table S-5b-d). Wing and Callahan empirically correlated the Mo−O−Mo bond angle and the vibrational frequency for mono-oxo bridged (Mo_2O_3) and dioxo-bridged (Mo_2O_4) species.[49] They assigned IR bands, reported by Colton and Rose at 735 and 516 cm^{-1} for $Cs_2[Mo_2O_3Cl_8]$,[20] as bridge vibrations, which would indicate a bent mono-bridged system with an Mo−O−Mo angle of ∼130°.

Mo K-Edge XANES Spectroscopy. The Mo K-edge XANES spectra of $MoCl_5$ solutions in different HCl concentrations as well as for the solid compounds **1**−**3** are shown in Figure 6. Details about the energies of the first inflection points (E_0) and the spectral features in the XANES region are presented in Table S-6. The first inflection point for the mononuclear $[MoOCl_5]^{2-}$ complex in **1** appears at 20 006.2 eV, while the second inflection point at 20 013.5 eV is similar to the reported value for $MoCl_5$, 20 014.3 eV.[50] The first inflection points for the mononuclear compound **2** and all Mo(V) solutions in HCl vary over the range 20 007.2−20 008.0 eV and are ∼1−2 eV higher than those of both **1** and **3** (Table S-6).

All 11 solutions as well as **2** and **3** show a shoulder at the onset of the rising absorption edge at ∼20 009 eV, which can easily be observed in the second derivative of the spectra. This characteristic feature for oxo-molybdenum complexes with an Mo═O bond is known as the "oxo-edge" transition and originates from a formally dipole forbidden (1s → 4d) transition to an antibonding state.[50−56] This feature appears as a distinct peak for **3** and for solutions with HCl concentration ≤ 4.5 M; however, it is very weak in the spectrum of **1**, $(HPPh_3)_2[MoOCl_5]$.

At the rising edge at ∼20 019 eV another growing shoulder appears, which becomes distinct for $MoCl_5$ solutions in HCl(aq) ≥ 4.9 M as well as for **1** and **2**. For molybdates (MoO_4^{2-}) such a transition has been described as "an inherent feature of continuum, a *p*-like resonance peak", rather than another bound-state transition.[55] This shoulder is weak in the XANES spectra of complex **3** and $MoCl_5$ solutions with HCl concentration ≤ 4.5. The intensity ratio between the two shoulders reverses with increasing HCl concentration, as shown by the second derivative of the spectra (Figure 6). The similarity between the XANES features of $MoCl_5$ in 7.4−9.4 M HCl with that of compound **2**, with four deep minima at about 20 009, 20 019, 20 032, and 20 042 eV in the second derivative (Figure S-5), supports our conclusion based on the position of the Mo−O stretching Raman bands that the dominating Mo(V) complex in these solutions is $[MoOCl_4(H_2O)]^-$ rather than $[MoOCl_5]^{2-}$. The Mo K-edge XANES spectra of $MoCl_5$ in ≤4.5 M HCl solutions are alike that of **3**, suggesting a similar dominating dinuclear dioxo-bridged complex, even though the second derivatives show that both peaks for **3** are at slightly lower energies (Figure 6). In the solid compounds **1**−**3**, large organic counterions prevent strong electrostatic interactions that could affect energy resolution or positions of the peaks and allow reliable comparisons between solutions and solid standards.

Mo K-Edge EXAFS Spectroscopy. The Mo K-edge EXAFS spectra and corresponding Fourier-transforms for $MoCl_5$ solutions in 1.7−9.4 M HCl and the compounds **1**−**3** are shown in Figure 3. The Fourier transforms for **1** and **2** as well as the $MoCl_5$ solutions in 4.9−9.4 M HCl exhibit two peaks at ∼1.3 Å and ∼2.0 Å (without phase shift correction), corresponding to the terminal Mo═O and Mo−Cl bonds, respectively. For **3,** and for $MoCl_5$ in less concentrated HCl(aq) solutions, ≤4.5 M, the first peak shifts

(49) Wing, R. M.; Callahan, K. P. *Inorg. Chem.* **1969**, *8*, 871.
(50) Cramer, S. P.; Hodgson, K. O.; Gillum, W. O.; Mortenson, L. E. *J. Am. Chem. Soc.* **1978**, *100*, 3398.
(51) Cramer, S. P.; Eccles, T. K.; Kutzler, F. W.; Hodgson, K. O. *J. Am. Chem. Soc.* **1976**, *98*, 1287.
(52) Jalilehvand, F.; Lim, B. S.; Holm, R. H.; Hedman, B.; Hodgson, K. O. *Inorg. Chem.* **2003**, *42*, 5531.
(53) George, G. N.; Kipke, C. A.; Prince, R. C.; Sunde, R. A.; Enemark, J. H.; Cramer, S. P. *Biochemistry* **1989**, *28*, 5075.
(54) Thapper, A.; Donahue, J. P.; Musgrave, K. B.; Willer, M. W.; Nordlander, E.; Hedman, B.; Hodgson, K. O.; Holm, R. H. *Inorg. Chem.* **1999**, *38*, 4104.
(55) Kutzler, F. W.; Natoli, C. R.; Misemer, D. K.; Doniach, S.; Hodgson, K. O. *J. Phys. Chem.* **1980**, *73*, 3274.
(56) Kutzler, F. W.; Scott, R. A.; Berg, J. M.; Hodgson, K. O.; Doniach, S.; Cramer, S. P.; Chang, C. H. *J. Am. Chem. Soc.* **1981**, *103*, 6083.

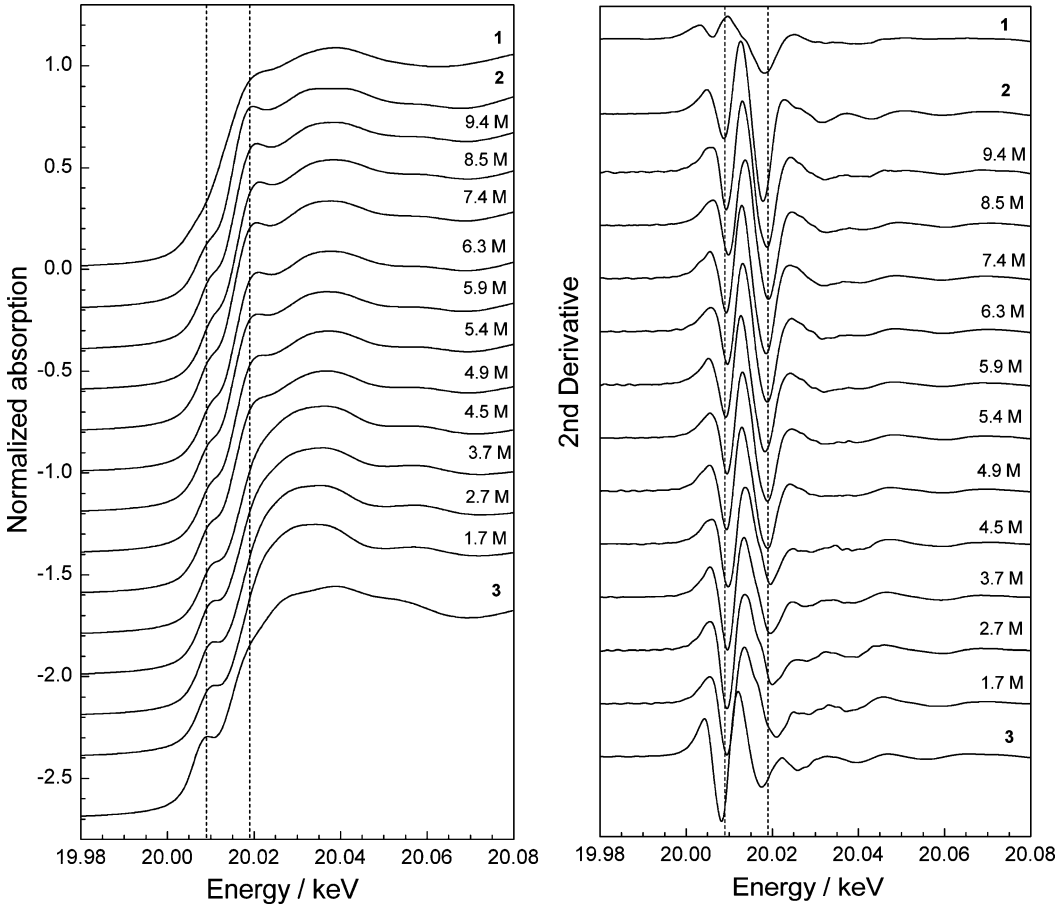

Figure 6. Normalized Mo K-edge XANES spectra for $MoCl_5$ in 1.7−9.4 M HCl solutions and the solid compounds **1**−**3**. The vertical dashed lines are at 20 009 and 20 019 eV (see Table S-6).

to ∼1.5 Å, and a new FT peak corresponding to the Mo−Mo interaction at ∼2.25 Å indicates the formation of a dinuclear species. When the number of aqua ligands around molybdenum increases, the Mo−Cl peak merges into the Mo−Mo peak in the Fourier transform.

As discussed in the Raman spectroscopy section, the $MoCl_5$ solutions in 7.4−9.4 M HCl show very similar Raman spectra and are dominated by the mononuclear $[MoOCl_4(H_2O)]^-$ complex. In 1.7 M HCl, however, a dioxo-bridged dinuclear complex with an Mo_2O_4 core dominates. At all intermediate HCl concentrations mixtures of Mo(V) complexes contribute to the Mo K-edge EXAFS oscillation, and the least-squares curve-fitting of these spectra will only provide an average of the bond distances for all Mo(V) species present in the solution. Therefore, only the Mo(V) solutions in 1.7−2.7 M and 7.4−9.4 M HCl and the reference compounds **1**−**3** were subjected to EXAFS least-square model curve-fitting. The results are shown in Figure 3 with the model parameters summarized in Table 2. For the $MoCl_5$ solutions in intermediate HCl concentrations (3.7−6.3 M) principal component analysis was used to establish the number of different major species present, followed by fitting linear combinations of reference spectra to determine the distribution of Mo(V) species in each solution (see below; also Appendix 6 in the Supporting Information).

The average molybdenum bond distances obtained from EXAFS analyses of **1**−**3** are in good agreement with those from crystal structures (see Table 2 and Figures 3 and 4). The EXAFS of **1**, crystalline $(HPPh_3)_2[MoOCl_5]$, fitted well with a model containing one Mo═O bond distance at 1.66(2) Å, four Mo−Cl at 2.40(2) Å, and one Mo−Cl at 2.55(2) Å, in agreement with corresponding bond distances in the crystal structure of **1,** 1.647 Å, 2.364−2.406 Å, and 2.563 Å, respectively.[17] The Debye−Waller (DW) parameter for the Mo═O back-scattering pathway was calculated to 0.0013 $Å^2$ using the program Feff 8.1,[25] for the force constant 758.6 $N\cdot m^{-1}$ of the Mo═O bond in **1**, with the Raman frequency of υ_{Mo-O} 969 cm^{-1} obtained in this study. In the refinement the DW parameter for the Mo═O path was fixed at the calculated value $\sigma^2 = 0.0013$ $Å^2$, otherwise the refinement resulted in a smaller value, 0.0007 $Å^2$.

Fitting of the k^3 weighted EXAFS oscillation of **2** resulted in one Mo═O bond distance at 1.66(2) Å, one Mo−OH_2 at 2.27(2) Å, and four Mo−Cl at 2.39(2) Å. These distances are comparable with the bond lengths obtained by X-ray crystallography: 1.641 Å, 2.278 Å, and 2.367−2.378 Å, respectively. The DW parameter for Mo═O was fixed at 0.0013 $Å^2$ (see above) and for Mo−OH_2 at 0.0030 $Å^2$ (the refined σ^2 value for the Mo−OH_2 bond distance 2.31(2) Å in **3** is 0.0032 $Å^2$). Refinements of the corresponding parameters for the Mo═O and Mo−OH_2 pathways resulted in small values, 0.0009 and 0.0011 $Å^2$, respectively.

The EXAFS spectra of the 0.2 M $MoCl_5$ solutions in 7.4−9.4 M HCl are indistinguishable (Figure S-6a) and also

overlap closely with the EXAFS oscillations of the mononuclear complex $[MoOCl_4(H_2O)]^-$ in **2** (Figure S-6c) but differ from the $[MoOCl_5]^{2-}$ complex in **1** (see Figure S-6d). The same pattern was also found for the Mo K-edge and $L_{2,3}$-edge (see below) XANES spectra of these solutions, in comparisons with corresponding XANES spectra of **1** (K-edge only) and **2**. Therefore, it can be concluded that the mononuclear Mo(V) complex in these solutions is $[MoOCl_4(H_2O)]^-$, rather than $[MoOCl_5]^{2-}$. This supports the earlier suggestion of Boorman et al. from ESR studies.[5]

Least-squares model curve-fitting of the EXAFS oscillations resulted for the 0.2 M $MoCl_5$ solutions in 7.4−8.5 M HCl in the average bond distances Mo═O 1.66(2) Å and Mo−Cl 2.38(2) Å, with DW parameters 0.0012 and 0.0045 Å^2, respectively, and in addition Mo−OH_2 2.30(2) Å (DW parameter fixed to 0.0030 Å^2) for the $[MoOCl_4(H_2O)]^-$ complex. Similar bond distances were obtained for the $MoCl_5$ solution in 9.4 M HCl (see Table 2).

The EXAFS model fitting for **3** resulted in the following distances: one Mo═O 1.67(2) Å, two μ-Mo−O 1.94(2) Å, two Mo−Cl 2.43(2) Å, one Mo−OH_2 2.31(2) Å, and one Mo−Mo interaction at 2.61(2) Å, which are in good agreement with the corresponding crystallographic distances: 1.68, 1.94, 2.45−2.48, 2.32−2.35, and 2.59 Å (Table 2 and Figures 3 and 4).

The 0.2 M $MoCl_5$ solution in 2.7 M HCl still shows a minor peak at 802 cm^{-1} in the Raman spectrum from the mono-oxo bridged dinuclear Mo(V) complex. However, its EXAFS oscillation is similar to that of the $MoCl_5$ solution in 1.7 M HCl with a dominating dioxo-bridged dinuclear Mo(V) species (Figure S-7a), which displays considerable phase shift differences from **3** (Figure S-7b).[37] EXAFS curve-fitting of the Mo(V) species in 1.7 M HCl with the structural model $[Mo_2O_4Cl_4(H_2O)_2]^{2-}$ (model *1* in Table 2) results in shorter Mo−OH_2 bond length (0.16 Å) and Mo−Mo distance (0.05 Å) than in **3**. However, the DW parameter for Mo−OH_2 shows a slight increase rather than the expected decrease, from 0.0032 Å^2 to 0.0038 Å^2. A concurrent increase in the average Mo−Cl bond length (0.04 Å) is accompanied with a drastic increase of its DW parameter from 0.0062 Å^2 to 0.0140 Å^2, corresponding to a wider distribution of the Mo−Cl bond distances (Table 2). Thus, the structure of the dinuclear Mo(V) species in dilute HCl solutions differs to some extent from that in **3**. For the interpretation, it should be noted that while the EXAFS technique provides precise distances (better than ± 0.02 Å) for strongly bonded interactions, the coordination numbers of the different types of chloro and aqua ligands in the Mo(V) species in 1.7 M HCl are less certain. For example, equally good fits are obtained for either $[Mo_2O_4Cl_3(H_2O)_3]^-$ with a ligand distribution of $[(OH_2)Cl_2OMo\text{-}(\mu\text{-}O)_2\text{-}MoOCl(OH_2)_2]^-$ (model *2* in Table 2) or for the neutral species $[Mo_2O_4Cl_2(H_2O)_4]$, which possibly is not soluble in aqueous solution. When increasing the number of water molecules, the bond distances do not change; however, the DW parameter for the Mo−OH_2 path increases from 0.0038 Å^2 (in model *1*) to σ^2 = 0.0056 Å^2 (model *2*) and 0.0068 Å^2, respectively.

A database survey showed 14 crystal structures with dioxo-bridged dinuclear molybdenum complexes corresponding to the general formula $[Mo_2O_4(H_2O)_2X_4]$, eight of which are bis-oxalato compounds and two polymeric structures.[57] In all the non-polymeric crystal structures, except the two chloro complexes **3** and $(NEt_4)[Mo_2O_4Cl_3(H_2O)_3]$, two aqua ligands occupy equatorial positions relative to the axial Mo═O bond, with the Mo−H_2O_{eq} bond lengths varying over a range of 2.113−2.197 Å. In the $(NEt_4)[Mo_2O_4Cl_3(H_2O)_3]$ compound there is also one Mo−H_2O_{eq} bond at 2.231 Å.[58] Aqua ligands in *trans*-position have only been found in the two above chloro complexes, with the Mo−H_2O_{trans} distances in the range of 2.335−2.408 Å. The strong *trans* influence of the Mo═O oxo group elongates and labilizes the opposite axial Mo-L bond.[5] A similar effect can be observed for the $[MoOCl_5]^{2-}$ complex in **1**, with four equatorial Mo−Cl bond distances at 2.36−2.41 Å and one *trans* Mo−Cl bond at 2.56 Å.[17] The crystallographic data base survey showed, besides complexes **3** and $(NEt_4)[Mo_2O_4Cl_3(H_2O)_3]$, only two other crystal structures containing an Mo_2O_4 core with chloro ligands in an equatorial position relative to the Mo═O group, $[Mo_2O_4Cl_2(1,10\text{-phen})_2]$ and $[Mo_2O_4Cl_2(dmbpy)_2]$,[59,60] where the Mo−Cl_{eq} distances vary from 2.43 to 2.48 Å.

A similar survey of 13 crystal structures containing the monomeric $[MoOCl_4(H_2O)]^-$ unit showed that the aqua ligand consistently prefers the *trans*-position to the Mo═O bond. The Mo−OH_2 bond distance varies between 2.285 and 2.393 Å.[57] No crystal structure was found with an aqua ligand in an equatorial position to the axial Mo═O bond in a mononuclear Mo(V) complex.

The short Mo−OH_2 distance of 2.15(2) Å, obtained from the Mo K-edge EXAFS analysis of 0.2 M $MoCl_5$ in 1.7 M HCl (in comparison with 2.31(2) Å in **3**), suggests that at this relatively low HCl concentration at least one aqua ligand replaces chlorine in the more strongly bonded equatorial position. The increase in the DW parameter (cf. Table 2) indicates some contribution from other Mo−OH_2 distances, e.g., from another aqua ligand in a *trans*-position to the Mo═O bond.

The mean Mo−Cl bond distance, 2.47(2) Å, and the DW parameter, σ^2 = 0.0125−0.0140 Å^2 (models *1* and *2* in Table 2), increase in comparison with **3**, for which all chloro ligands are in equatorial positions with Mo−Cl 2.43(2) Å and σ^2 = 0.0062 Å^2. This implies larger variation in the Mo−Cl bond lengths, e.g., with a chloro ligand *trans* to the Mo═O bond. Probable structures for Mo(V) species in equilibrium in 1.7 M HCl are shown in Scheme 1 (complex ***a*** is similar to that in **3**).

According to our gas-phase ADF calculations of the total energies for the isomeric structures ***a***−***c*** with the composition $[Mo_2O_4Cl_4(H_2O)_2]^{2-}$, ***a*** (from the crystal structure of **3**) and ***b*** would be the most stable ones (−87.6 and −86.9 eV,

(57) Cambridge Structural Database (CSD); Version 1.7, 2004 release. Allen, F. H. *Acta Crystallogr., Sect. B: Struct. Sci.* **2002**, *B58*, 380.
(58) Khan, M. I.; Chen, Q.; Zubieta, J. *Inorg. Chim. Acta* **1995**, *235*, 135.
(59) Xu, L.; Wang, E.; Hu, C.; Huang, R. *Transition Met. Chem. (Dordrecht, Neth.)* **2001**, *26*, 563.
(60) Dulebohn, J. I.; Stamatakos, T. C.; Ward, D. L.; Nocera, D. G. *Polyhedron* **1991**, *10*, 2813.

Scheme 1. Probable Structures (***b*** and ***d*** are the Major Species) of Dioxo-Bridged Dinuclear Mo(V) Complexes in $MoCl_5$ Solution in 1.7 M HCl

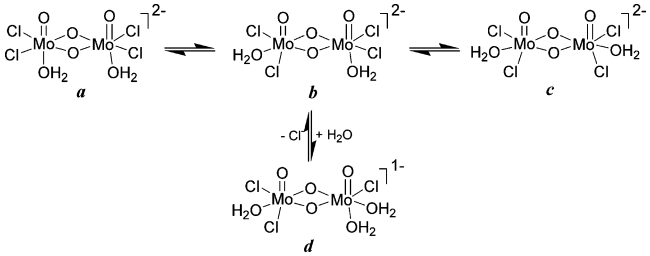

respectively). Structure ***c*** with higher total energy, −85.8 eV, is likely to be less stable because of the strain associated with the repulsion between the two chloro ligands *trans* to the Mo═O bond (the sum of the van der Waals' radii for two chlorine atoms is ∼3.6 Å and the Mo−Mo distance is 2.56(2) Å; see Appendix 9, Supporting Information and Figure S-17). The structural differences between the Mo(V) coordination in compound **3** and in 1.7 M HCl are also reflected in their Mo $L_{2,3}$-edge XANES spectra and in the theoretical calculations for the dioxo-bridged Mo(V) species in Scheme 1.

Principal Component Analysis (PCA). The Raman spectra of the $MoCl_5$ solutions in 1.7−9.4 M HCl show three categories of Mo(V) species: mononuclear, mono-oxo bridged (Mo_2O_3 core), and dioxo-bridged (Mo_2O_4 core) dinuclear complexes. While the 1.7−2.7 M and 7.4−9.4 M HCl solutions are dominated by the dioxo-bridged dinuclear and mononuclear Mo(V) complexes, respectively, solutions with intermediate HCl concentration, 3.7−6.3 M, contain a mixture of species.

PCA analysis of EXAFS spectra, however, can only distinguish two major types of components (see Appendix 6, Supporting Information). As shown in Figure S-12 and Table S-7, component **I** dominates for solutions with HCl concentrations ≥ 4.9, with a negligible contribution from component **II** to the k^3-weighted EXAFS oscillations for Mo(V) solutions in 5.4−6.3 M HCl. For more dilute HCl solutions, ≤4.5 M, component **II** dominates. This is consistent with the distinct change observed in the Fourier-transform of the EXAFS spectra of dilute HCl solutions (≤4.5 M) (see Figure 3) and in the Mo $L_{2,3}$-edge XANES spectra (see below), where the $MoCl_5$ solutions in 4.9−9.4 M HCl showed three absorption peaks and only two peaks below 4.5 M HCl (see Figure 8).

The above analysis shows that the EXAFS technique is not able to separate the contribution of the mono-oxo bridged Mo(V) complex as one distinguishable major component in the intermediate HCl concentration range (3.7−6.3 M). The distinct Raman band at ∼802 cm^{-1} indicates the presence of the dinuclear mono-oxo bridged Mo(V) complex in solutions with 2.7 M < c_{HCl} ≤ 6.3 M (see Figure 5), and the UV−vis absorption at λ_{max} = 726 nm shows that it has the highest concentration in 0.2 M $MoCl_5$ in 4.9 M HCl (see Figure S-1). However, no clear estimate of the amount is available. Hare et al. proposed the highest concentration, ∼25−30%, for such a dimer at 6 M HCl,[6] while Lincoln and Loehr reported Raman band assignments for 0.163 M

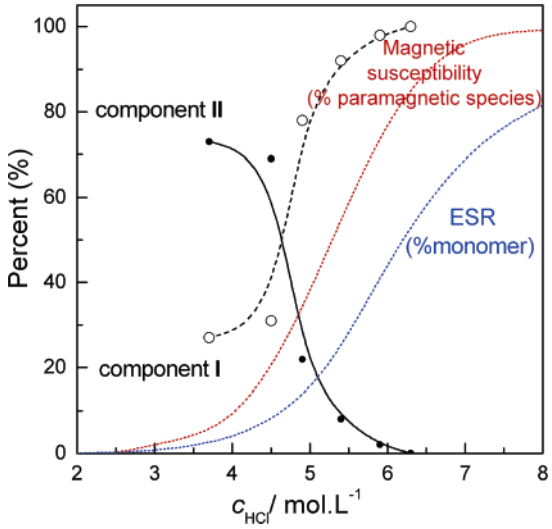

Figure 7. Distribution of the two PCA components for the Mo K-edge EXAFS spectra of 0.2 M $MoCl_5$ solutions in 3.7−6.3 M HCl(aq) (see model *1*, Table S-7). The components represent the $MoCl_5$ solution in 7.4 M HCl (= component **I**) and a dinuclear dioxo-bridged Mo(V) complex similar to **3** (= component **II**). The results are compared with ESR measurements of the amount of MoO^{3+} monomer with $[Mo^V]$ = 0.03 M in various HCl concentrations (prepared by dissolving $(NH_4)_2[MoOCl_5]$ ref 6) and magnetic susceptibility measurements for HCl(aq) solutions with $[Mo^V]$ = 0.33 M (prepared by reducing molybdic acid in concentrated HCl; ref 3). Note that the different preparations in the three studies lead to some differences in the actual total $[H^+]$ and $[Cl^-]$ concentration, according to reactions 1 and 3.

$[Mo_2O_3Cl_8]^{4-}$ in 6 M HCl, assuming all Mo(V) to be in a mono-oxo bridged dimer.[12] In the current study, the k^3-weighted EXAFS oscillation of the 0.2 M $MoCl_5$ solution in 5.9 M HCl fits in least-squares curve-fitting very well with a model similar to that for the 7.4−9.4 M solutions, comprising one Mo═O, one Mo−OH_2, and four Mo−Cl bond distances, at 1.66(2), 2.31(2), and 2.38(2) Å, respectively. Attempts to fit a mononuclear or mono-oxo bridged Mo(V) model to the k^3-weighted EXAFS oscillation of the 0.2 M $MoCl_5$ solution in 4.9 M HCl failed.

When interpreting the amount of component **I** only in terms of mononuclear species, such as the $[MoOCl_4(H_2O)]^-$ complex in **2** (in models *2* and *3* in Table S-7) or that in 0.2 M $MoCl_5$ in 7.4 M HCl (in model *1* in Table S-7), this type will become overestimated in the EXAFS results, especially in a comparison with the distribution of MoO^{3+} monomeric species from a more specific method such as the ESR studies by Hare et. al for 0.030 M Mo(V) solutions, prepared by dissolving $(NH_4)_2[MoOCl_5]$ solid in various HCl concentrations (see Figure 7).[6] For example, from the ESR studies the estimated amounts of the monomeric and the mono-oxo bridged Mo(V) complexes in 6 M HCl were 46% and ∼25−30%, respectively, i.e., the sum is ∼70−75%,[6] while the amount of component **I** in 0.2 M $MoCl_5$ in 5.9 M HCl was obtained as ∼95%. One would expect that the higher metal ion concentration in the current study (0.2 M $MoCl_5$) would enhance the formation of dinuclear species.

The observed trend in how the amount of component **I** changes resembles the previously reported sudden change in magnetic properties of 0.33 M Mo(V) solutions that occurs around ∼5.5 M HCl (see Figure 7).[3] In those solutions that

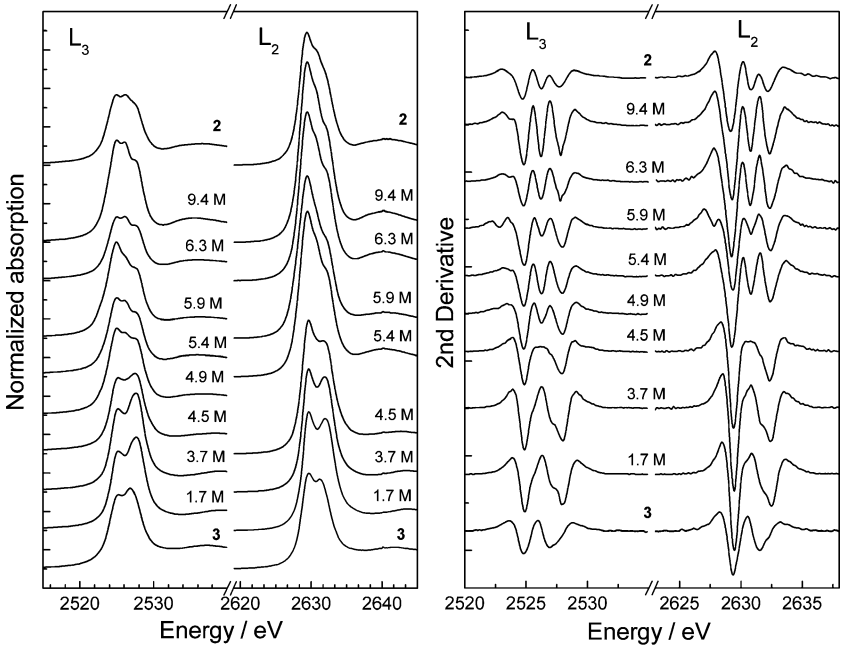

Figure 8. (left) Normalized Mo $L_{2,3}$-edge XANES spectra of 0.2 M $MoCl_5$ in 1.7−9.4 M HCl solutions and of the solid compounds **2** and **3** and (right) corresponding second derivatives (for the position of minima, see Table S-9). The spectra were normalized to their edge steps, which were consistently larger for L_3-edges than for L_2. Consequently, the normalized L_2-edge features appear larger than the normalized L_3-edges.

were prepared from a stock Mo(V) solution made by reducing the molybdic acid in concentrated HCl, the higher Mo(V) concentration than in the current study (0.2 M) would promote the formation of diamagnetic dinuclear Mo(V) species. Also, the Mo(V) source was dissolution of $MoCl_5$ in the present study, which provides higher total chloride concentration, promoting the mononuclear complex (cf. reaction 1).

The PCA analysis indicates that component **I** represents all Mo(V) species without a double oxo bridge, including the mononuclear complex and all mono-oxo bridged Mo_2O_3 entities, while component **II** corresponds to dioxo-bridged dinuclear species with an Mo_2O_4 core and a distinct Mo−Mo distance. The later assumption is supported by the comparison of the Fourier-transform of component **II** with that of 0.2 M $MoCl_5$ in 1.7 M HCl (see Figure S-11). The comparison of the Fourier-transform of component **I** with that of 0.2 M $MoCl_5$ in 7.4 M HCl (Figure S-10a) shows that the peak at ∼2 Å, which corresponds to Mo−Cl and Mo−OH_2 bond distances, has smaller amplitude and is shifted slightly toward shorter distances. This would indicate that the mono-oxo bridged complex gives rise to an EXAFS oscillation only slightly different from the mononuclear $[MoOCl_4(H_2O)]^-$ complex in **2**.

Nonlinear Mo_2O_3 Species. According to reaction 1, the first mono-oxo bridged dinuclear Mo(V) complex formed in HCl solutions as hydrolysis product of $[MoOCl_4(H_2O)]^-$ is $[Mo_2O_3Cl_6(OH_2)_2]^{2-}$. The EXAFS oscillation for this species was simulated considering two different options (see Appendix 7): a "nonlinear" and a "linear" Mo−O−Mo entity (based on a model shown in Figure S-13). For a $[Mo_2O_3Cl_6(OH_2)_2]^{2-}$ complex with a "linear" or "near-linear" Mo−O−Mo group (for Mo−O−Mo angles > 150°), a simulation only based on the single-scattering paths (Mo═O, Mo−O_b, Mo−OH_2, and Mo−Cl) resulted in an EXAFS oscillation (see Figure S-14 left, A), which was to some extent similar to that of component **I**. When adding the Mo−O−Mo multiple scattering path (Figure S-14, left, B), the "focusing-effect" within this pathway drastically enhances the multiple scattering contribution and introduces a complex oscillation pattern. Also, a distinct peak appears at ∼3.3−3.4 Å in the Fourier-transform, corresponding to the Mo−O−Mo distance ∼3.7 Å for a linear entity, as in the crystal structure of $[Mo_2O_3Cl_4(py)_4]\cdot CH_2Cl_2$.[61] Such an FT peak is not observed for component **I** (see Figure S-10a).

Even though all reported crystal structures with an Mo_2O_3 core have linear diamagnetic Mo−O−Mo bridges, a non-linear bridge is needed to explain the paramagnetic mono-oxo bridged dinuclear species proposed in HCl solutions. Hence, the EXAFS oscillation was modeled with a "non-linear" Mo−O−Mo bridge (Mo−O−Mo < 150°) in case C, keeping the same Mo═O and Mo−Cl bond distances except for the Mo−O_b bond distance 1.93 Å in the bridge, which was equal to Mo−O_b in **3** (Figure S-14 C). Since the two molybdenum ions in that model are not rigidly joined, a high DW parameter would be expected for the Mo−Mo distance, rapidly damping out that EXAFS contribution. The simulated EXAFS (and the corresponding Fourier-transform) for the "nonlinear" model (case C) resembles the k^3-weighted EXAFS of 0.2 M $MoCl_5$ in 7.4 M HCl and of **2**, especially that of 0.2 M $MoCl_5$ in 4.9 M HCl, which according to the UV−vis spectra, contains the highest concentration of the mono-oxo bridged complex. Hence, component **I** can be considered as a combination of the EXAFS oscillations of a "nonlinear" mono-oxo bridged and a mononuclear complex, e.g., $[Mo_2O_3Cl_6(OH_2)_2]^{2-}$ and $[MoOCl_4(H_2O)]^-$.

(61) El-Essawi, M. M.; Weller, F.; Stahl, K.; Kersting, M.; Dehnicke, K. *Z. Anorg. Allg. Chem.* **1986**, *542*, 175.

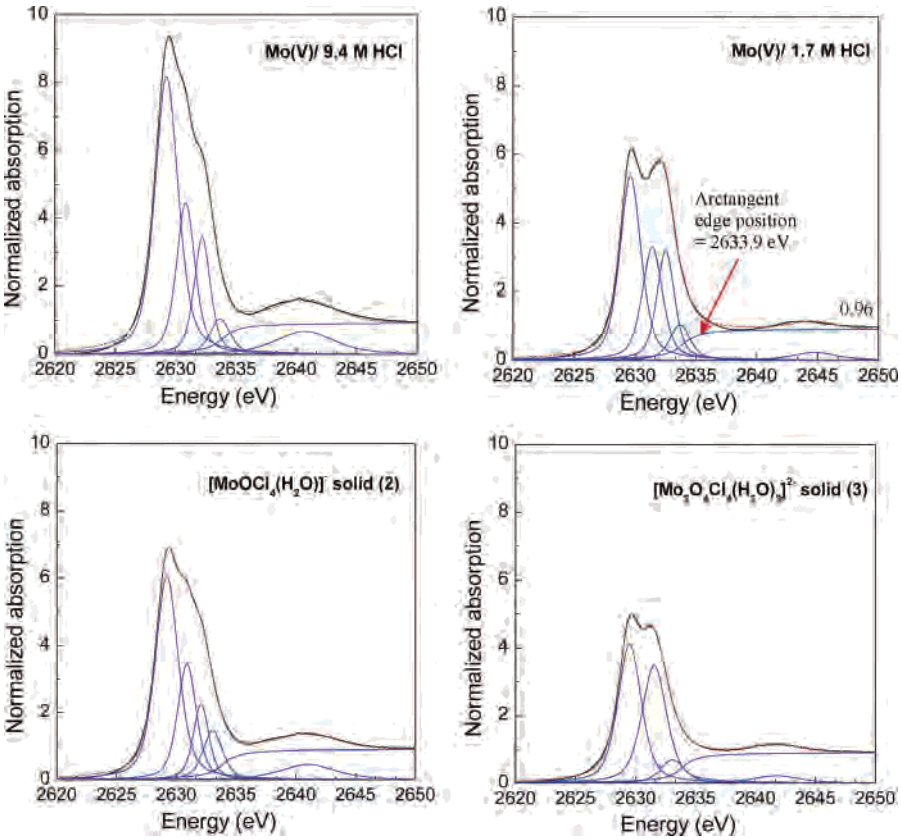

Figure 9. Peak-fitting of Mo L_2-edge absorption features (50:50 Gaussian + Lorentzian) for solids **2** and **3** and 0.2 M $MoCl_5$ solutions in 1.7 and 9.4 M HCl, with fit (- - -) (red) and deconvoluted peaks (—) (blue), using the EDG_FIT program in EXAFSPAK (see Table 4). The arctangent edge position was fixed at 2633.9 eV with an amplitude of 0.96 for all solutions. The position of the deconvoluted peaks varied up to 0.2 eV, when varying the arctangent edge position within ±5 eV.

In a careful vibrational spectroscopic study, Lincoln and Loehr suggested that $[Mo_2O_3Cl_8]^{4-}$ dominates for Mo(V) solutions in 5−6 M HCl.[12] They assigned a vibrational band at ~380 cm^{-1} as the symmetric Mo−O−Mo stretching of a linear bridge. However, their suggestion "The greater than expected ^{18}O-isotope shift for a linearly bridged system could suggest that the predicted C_{2h} or C_{2v} symmetry of the $Mo_2O_3^{2+}$ species in 6 M HCl may not hold perfectly in solution"[12] is consistent with the current EXAFS results.

Mo L-Edge XANES Spectroscopy. Mo L_2- and L_3-edges originate from the 2p core level, and their 105 eV energy separation results from 2p spin−orbit coupling. While the dipole allowed transitions at the K-edge are restricted to 1s → *n*p, with an intensity expected to be proportional to the p character of the receiving unoccupied molecular orbital, at the $L_{2,3}$-edge electronic transitions with both 2p → *n*s and 2p→ *n*d character are dipole allowed. The spectral features at the $L_{2,3}$-edge are better resolved, since the natural core-hole line width for the $L_{2,3}$- edge is about three times sharper than that of the K-edge.[62] Intense "white-lines" at the Mo L_2- and L_3-edges are due to $2p_{1/2}$ → 4d and $2p_{3/2}$ → 4d transitions, respectively, and the fine splitting of their spectral shapes results from the ligand-field splitting of the d-orbitals,[63] which makes this technique a useful tool to probe the ligand field energies and coordination geometry of the central molybdenum atom in its complexes.[62,64−66]

The relative intensities of the peaks generally reflect the probability of the transitions.[63] Since there are four electrons at the $2p_{3/2}$ level and two electrons at the $2p_{1/2}$ level, the intensity ratio between the L_3 and L_2 edges would be expected to be close to 2:1. However, the relative intensity ratios of the L_3- to L_2-edges are less than 2:1 for all the Mo-(V) samples in this study, as shown in Figure S-15. Changes in relative peak intensities, when comparing the L_3 edge to the L_2 edge for 4d transition metals, have been attributed to the 4d spin−orbit coupling and 2p-4d multiplet effects, i.e., overlapping interactions between the radial wave functions of the core 2p-hole and the valence 4d-hole.[67−69] For the 4d elements the magnitude of such effects is smaller than the 2p spin−orbit coupling, and intensity transfer from the L_3-

(62) George, G. N.; Cleland, W. E., Jr.; Enemark, J. H.; Smith, B. E.; Kipke, C. A.; Roberts, S. A.; Cramer, S. P. *J. Am. Chem. Soc.* **1990**, *112*, 2541.

(63) Hedman, B.; Frank, P.; Gheller, S. F.; Roe, A. L.; Newton, W. E.; Hodgson, K. O. *J. Am. Chem. Soc.* **1988**, *110*, 3798.

(64) Izumi, Y.; Glaser, T.; Rose, K.; McMaster, J.; Basu, P.; Enemark, J. H.; Hedman, B.; Hodgson, K. O.; Solomon, E. I. *J. Am. Chem. Soc.* **1999**, *121*, 10035.

(65) Evans, J.; Mosselmans, J. F. *J. Phys. Chem.* **1991**, *95*, 9673.

(66) Fronzoni, G.; Stener, M.; Reduce, A.; Decleva, P. *J. Phys. Chem. A* **2004**, *108*, 8467.

(67) de Groot, F. M. F.; Hu, Z. W.; Lopez, M. F.; Kaindl, G.; Guillot, F.; Tronc, M. *J. Chem. Phys.* **1994**, *101*, 6570.

(68) de Groot, F. *Coord. Chem. Rev.* **2005**, *249*, 31.

(69) Sham, T. K. *J. Am. Chem. Soc.* **1983**, *105*, 2269.

Table 4. Deconvoluted Peak Energy for Mo L_2-Edge Absorption Spectra[a]

	sample	peak	*1*	*2*	*3*	*4*
(A)	solid **2**	energy	2629.2	2630.9	2632.1	2633.1
		from peak 1	0	1.7	2.9	3.9
		fwhh	1.13	0.91	0.78	0.97
(B)	9.4 M HCl	energy	2629.2	2630.8	2632.2	2633.2
		from peak 1	0	1.6	3.0	4.0
		fwhh	1.14	0.90	0.79	0.86
(C)	solid **3**	energy	2629.5	2631.6		2633.1
		from peak 1	0	2.1		3.6
		fwhh	1.15	1.21		1.21
(D)	1.7 M HCl	energy	2629.6	2631.4	2632.5	2633.7
		from peak 1	0	1.8	2.9	4.1
		fwhh	1.03	0.99	0.85	0.99

[a] See Figure 9. 50% (Gaussian + Lorentzian) was used for curve-fitting of absorption peaks. The arctangent edge position was fixed at 2633.9 eV with an amplitude of 0.96 for all samples. (fwhh = full width at half height.)

to the L_2-edge does not occur in the same way as seen for 3d elements. However, such effects can still affect the spectral shapes of these edges, especially that of the L_3-edge,[62,64] thus making L_2-edge features more reliable for analysis.

Normalized Mo $L_{2,3}$-edge XANES spectra and their second derivatives for the Mo(V) solutions and the reference compounds **2** and **3** are shown in Figure 8, with the minima in the second derivative summarized in Table S-9. The results from peak fitting for the L_2-edge spectra of $MoCl_5$ solutions in 1.7 and 9.2 M HCl, and the compounds **2** and **3** are shown in Figure 9 and Table 4. While only two major peaks are resolved in the $L_{2,3}$-edges for $MoCl_5$ solutions in ≤4.5 M HCl, three peaks appear for higher HCl concentrations. Those features originate from the ligand field splitting of the Mo d-orbitals and indicate a major ligand field and/or geometry change around the molybdenum center (Figure 8).

For the $MoCl_5$ solution in 1.7 M HCl, at the L_3-edge the second peak at higher energy (~2527 eV) has higher intensity, while at the L_2-edge the first peak at lower energy (~2629 eV) is the more intense. Similar spectral shapes at the $L_{2,3}$-edges are observed for **3** (Figure 8). For molybdenum compounds in an octahedral ligand field, the intensity ratio of the first peak ($2p \rightarrow t_{2g}$) to the second ($2p \rightarrow e_g$) is often lower for the L_3-edge than for L_2.[63,64]

Our ADF calculations for the ground-state electronic structure of the $[Mo_2O_4Cl_4(trans\text{-}H_2O)_2]^{2-}$ complex of **3** show that the HOMO (75A), which has a significant amount (~55%) of Mo($4d_{xy}$) character, is occupied with two electrons due to the Mo−Mo bond formation.[18] The LUMO (76A) and LUMO+1 (77A), both with more than 50% mixed $4d_{xz}$ and $4d_{yz}$ character, are almost degenerate with only 0.2 eV energy difference (see Figure 10). Therefore, the first intense peak observed in the $L_{2,3}$-edge XANES spectra of **3** should correspond to the transition: Mo (2p) → [76A, 77A (d_{xz}, d_{yz})] (cf. Figures 8 and 9).

The experimentally observed splitting between the two peaks in the $L_{2,3}$-edge spectra of **3** is about 2.2 eV (the second derivative of the L_3-edge show a split of 2.1 eV and the L_2-edge 2.3 eV; cf. Figure 8 and Table S-9). This is comparable to the calculated energy difference of ~2.0 eV between the almost degenerate MOs 76A/77A, and 83A, which has about 50% Mo($4d_{x2-y2}$) character (Figure 10). Thus, the second intense peak observed in the $L_{2,3}$-edge absorption spectra of **3** should correspond to the transition: Mo(2p) → 83A(d_{x2-y2}) (cf. Figures 8 and 10). At the L_2-edge of **3** the third transition at 2633.1 eV (Figure 9) would contain the higher energy transitions 2p → 85A (with Mo 5s character), and 2p → 88A Mo($4d_{z2}$) according to the calculated energy differences in Figure 10 and the selections rules for dipole allowed electronic transitions at the L_2-edge (2p → *n*s and 2p→ *n*d).

In the present comparison between calculated and experimental energy differences one should keep in mind that the decreased shielding due to the core hole created at a transition will affect the energy levels somewhat differently for different types of the receiving molecular orbitals. The calculated energy differences between ground-state MO energy levels do not account for such relaxation effects nor that the receiving MOs momentarily after the electronic transition will be in a higher excited vibrational state.

As shown in Figure 8, the $L_{2,3}$-edge spectra of **3** differ from those of $MoCl_5$ in 1.7 M HCl solution. Their first peaks at the L_2-edge in Figure 9 (2629.5 and 2629.6 eV, respectively, cf. Table 4) are assigned as the 2p → (d_{xz}, d_{yz}) transition. The difference between the next absorption peaks, where the 2p → d_{x2-y2} and 2p → d_{z2} transitions occur (Figure 10), can be explained by comparing the local structure around the Mo(V) ions using Mo K-edge EXAFS (see Table 2). For the dinuclear Mo(V) complex in 1.7 M HCl the mean Mo−OH_2 bond distance is 0.16 Å shorter than in **3**, while the Mo−Cl bonds are only slightly longer (0.04 Å). That should result in a stronger octahedral ligand field and, therefore, a larger gap between the t_{2g} and e_g groups of orbitals. Only for the $[Mo_2O_4Cl_3(H_2O)_3]^-$ complex (***d***) our ADF calculations indicate a larger ligand field splitting (the increase is about 0.2 eV from ***a*** to ***b*** to ***d***, Figures 10 and S-17). Thus, the L_2-edge spectrum for the 1.7 M HCl solution indicates a significant contribution from structure ***d*** in the mixture of dioxo-bridged Mo(V) species.

In the UV−vis absorption spectrum of $MoCl_5$ in 1.7 M HCl, the peak at 389 nm (3.19 eV) cannot be due to a d−d transition, because the electrons are paired in the HOMO (d_{xy}) orbital; it is probably a charge-transfer band (see Figure S-1).

The three major transitions observed in the Mo $L_{2,3}$-edge spectra of **2** and of $MoCl_5$ in HCl(aq) concentrations between 4.9 and 9.4 M become more distinct in their second derivatives (Figure 8). In the $L_{2,3}$-edge spectra of **2**, the energy differences from peak *1*, to peaks *2* and *3* (the second and third minima in the second derivative) are found to be the same for both the L_2 and L_3-edges (1.6 and 3.0 eV, respectively), indicating similar electronic transitions originating from the $2p_{1/2}$ and $2p_{3/2}$ levels (Table S-9). This is in contrast with the previously reported unequal differences, 1.21, 2.83 eV at the L_3-edge and 0.58, 2.37 eV at the L_2-edge, for $[N(Et)_4][MoOCl_4(OH_2)]$.[62] For the $MoCl_5$ solution in 9.4 M HCl and for **2**, their three minima in the second derivative of the $L_{2,3}$-edge spectra appear with only ~0.1 eV difference (see Table S-9). Also their Mo XANES spectra

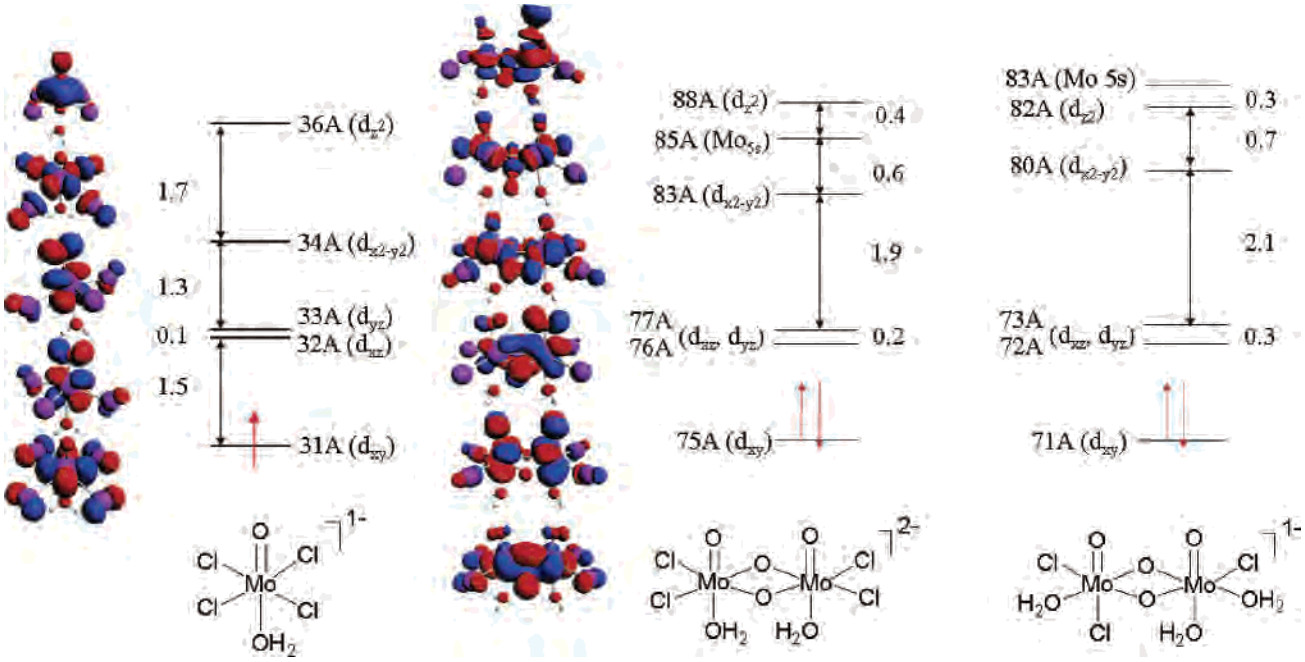

Figure 10. MO diagrams for the reference complexes $[MoOCl_4(H_2O)]^-$ in **2**, $[Mo_2O_4Cl_4(trans\text{-}H_2O)_2]^{2-}$ in **3**, and $[Mo_2O_4Cl_3(H_2O)_3]^-$ as one of the two major species in 1.7 M HCl.

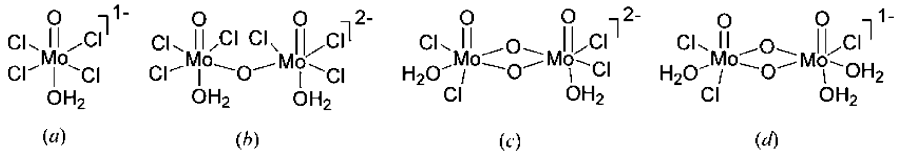

Figure 11. Major species in the investigated 0.2 M $MoCl_5$ solutions in (*a*) 6.3−9.4 M HCl, (*b*) 4.9−5.9 M HCl, and (*c*, *d*) 1.7−4.5 M HCl.

at the K-edge are very similar and strongly suggest that the dominating mononuclear complex in this solution is $[MoOCl_4(H_2O)]^-$.

Deconvolution of the features at the L_2-edge absorption spectra of **2** and of $MoCl_5$ in 9.4 M HCl, however, resulted in 4 peaks in the XANES region with ∼0.1 eV difference between corresponding peak positions (Figure 9 and Table 4). To interpret these transitions we have used results from ADF calculations. For the $[MoOCl_4(H_2O)]^-$ complex (without symmetry according to the crystal structure), the single valence electron ($4d^1$) of Mo(V) is located in an antibonding π^* molecular orbital with mainly $4d_{xy}$ character (62% Mo d_{xy}, 36% Cl 3p) (see Figure 10 and Table S-11). This is consistent with the previously reported theoretical calculations for the $[MoOCl_4(H_2O)]^-$ complex treated in C_{2v} symmetry, where the singly occupied molecular orbital (SOMO) was d_{x2-y2} with 62% Mo d and 35% Cl p character.[70,71] The present calculations indicate that the four peaks in the L_2-edge spectrum of **2** correspond to MO transitions with the following characters: $2p \rightarrow d^1_{xy}$, $2p \rightarrow d_{xz,yz}$, $2p \rightarrow d_{x2-y2}$ and $2p \rightarrow d_{z2}$, according to the calculated energy differences: 1.5 eV ($d_{xy} \rightarrow d_{xz,yz}$), 2.9 eV ($d_{xy} \rightarrow d_{x2-y2}$) and 4.6 eV ($d_{xy} \rightarrow d_{z2}$). These theoretical values are in fair agreement with the energy differences found experimentally between the peaks *2*−*4* and peak *1* (1.7, 2.9, and 3.9 eV, respectively) in the L_2-edge spectrum of **2** (see Table 4).

In the single-crystal UV−vis electronic absorption spectrum of $(AsPh_4)[MoOCl_4(H_2O)]$, two low-energy transitions have been reported at 13 400 cm^{-1} (746 nm, 1.66 eV) and 22800 cm^{-1} (439 nm, 2.83 eV),[72] very close to the energy differences between the peaks found in the L_2-edge spectrum of **2** (1.7 and 2.9 eV, see above). The 13 400 cm^{-1} transition is described as the electronic transition $d_{xy} \rightarrow d_{xz}$, d_{yz} (in C_{4v} symmetry)[72−74] or $d_{x2-y2} \rightarrow d_{xz}$, d_{yz} (in C_{2v} symmetry).[70,71] However, different assignments have been proposed for the transition at 22 800 cm^{-1}, i.e. $4d_{xy}^* \rightarrow 4d_{x2-y2}^*$ (C_{4v})[71,74] or $e(4d_{xz,yz}$, Mo−O $\pi) \rightarrow b_2^*(4d_{xy}$, Mo−Cl $\pi^*)$.[72] The energy of the $d_{xy} \rightarrow d_{z2}$ transition was calculated to ∼35550 cm^{-1} (4.4 eV),[71] while the peak-fitting of the L_2-edge of **2** shows about 3.9 eV. Thus, our current results support the assignment $4d_{xy} \rightarrow 4d_{x2-y2}$ for the 22800 cm^{-1} transition. This is similar to the assignment that Gray and Hare proposed for the 23000 cm^{-1} (434 nm) band in the reflectance spectrum of the $(NH_4)_2[MoOCl_5]$ compound.[4]

(70) Swann, J.; Westmoreland, T. D. *Inorg. Chem.* **1997**, *36*, 5348.
(71) Deeth, R. J. *J. Chem. Soc., Dalton Trans.* **1991**, 1895.
(72) Garner, C. D.; Hill, L. H.; Mabbs, F. E.; McFadden, D. L.; McPhail, A. T. *J. Chem. Soc., Dalton Trans.* **1977**, 1202.
(73) Garner, C. D.; Lambert, P.; Mabbs, F. E.; King, T. J. *J. Chem. Soc., Dalton Trans.* **1977**, 1191.
(74) Collison, D. *J. Chem. Soc., Dalton Trans.* **1990**, 2999.

Conclusions

The structure of the mononuclear Mo(V) complex in 7.4−9.4 M HCl was found to be $[MoCl_4(H_2O)]^-$ rather than $[MoOCl_5]^{2-}$, based on the similarity between the Mo K- and $L_{2,3}$-edge XANES spectra of these solutions and those of the $[MoOCl_4(H_2O)]^-$ complex in **2**. The Mo K- and $L_{2,3}$-edge X-ray absorption spectra revealed some differences between the structures of the dinuclear species in 0.2 M $MoCl_5$ solution in 1.7 M HCl and that of crystalline $(pyH)_2$-$[Mo_2O_4Cl_4(H_2O)_2]$ (**3**). While the aqua ligands in **3** are *trans* to the two axial Mo═O bonds (Mo−OH_2 2.31 Å), in solution at least one aqua ligand has replaced chlorine in an equatorial position to give Mo−OH_2 2.15 Å, e.g. as in the $[Mo_2O_4Cl_3(H_2O)_3]^-$ complex (Figure 11d).

In the Raman spectra of solutions with 2.7 M $\leq c_{HCl} \leq$ 6.3 M, an intense band characterizing a mono-oxo bridged complex with an Mo_2O_3 core appeared at 802 cm^{-1} (assigned as υ_{as} Mo−O−Mo) with the highest intensity between 4.5 M $\leq c_{HCl} \leq$ 5.9 M. In the UV−vis spectra the highest absorption at $\lambda = 726$ nm occurred for 0.2 M $MoCl_5$ in 4.9 M HCl, indicating the highest concentration of the mono-oxo bridged complex. The Mo K- and $L_{2,3}$-edge XANES spectra changed abruptly from 4.9 to 4.5 M HCl, and a new peak corresponding to a direct Mo−Mo interaction appeared in the Fourier-transformed Mo K-edge EXAFS spectra of 0.2 M $MoCl_5$ solutions with $c_{HCl} \leq 4.5$ M. PCA analysis of the EXAFS spectra of $MoCl_5$ solutions in 3.7 M $\leq c_{HCl} \leq$ 6.3 M could only distinguish two major components, one of which is similar to the EXAFS spectrum of Mo(V) in 7.4 M HCl or **2**, with the mononuclear $[MoCl_4(H_2O)]^-$ complex, and the other resembles the EXAFS spectrum of the $MoCl_5$ solution in 1.7 M HCl with dioxo double bridged species. Thus, even PCA analysis of the EXAFS data could not separate the contribution from the mono-oxo bridged dimeric Mo(V) species (such as $[Mo_2O_3Cl_6(OH_2)_2]^{2-}$) from that of the monomeric $[MoCl_4(H_2O)]^-$ complex. The main reason is probably that the EXAFS contributions become too similar because of a flexible single Mo−O−Mo bridge, which supports a "nonlinear" paramagnetic Mo−O−Mo structure that previously has been suggested to explain magnetic susceptibility measurements.[6] Furthermore, the EXAFS oscillations display no noticeable "focusing effect" that would in a linear or near-linear Mo−O−Mo entity (with Mo−O−Mo angle >150°) enhance the multiple-scattering contribution of this pathway. Also, no FT peak around 3.3−3.4 Å (without correction for phase shift), corresponding to the expected linear Mo−O−Mo distance at ∼3.7 Å, could be observed for any $MoCl_5$ solution in intermediate HCl concentrations.

Proposed structures for the major mononuclear and dioxo-bridged dinuclear Mo(V) species as well as the first mono-oxo bridged species formed in 0.2 M $MoCl_5$ solutions in different HCl concentrations are shown in Figure 11.

Acknowledgment. We are grateful to Prof. Benjamin C. Bostick (Dartmouth College, Hanover, U.S.A.) for measuring the EXAFS spectrum of **1**, Dr. Stephen R. Wasserman (Structural GenomiX Inc., Argonne National Laboratory) and Prof. Janos Mink (Chemical Research Center of the Hungarian Academy of Sciences, Budapest) for helpful discussions, and Prof. Tom Ziegler and Dr. Michael Seth (University of Calgary) for the use of the COBALT ADF cluster. X-ray absorption measurements were carried out at the Photon Factory, Tsukuba, Japan (proposal no. 2003G286) and Stanford Synchrotron Radiation Laboratory (SSRL), a U.S. national user facility operated by Stanford University on behalf of the U.S. Department of Energy, Office of Basic Energy Sciences (proposal no. 2848). We gratefully acknowledge the Natural Sciences and Engineering Council (NSERC) of Canada, Canadian Foundation of Innovations (CFI), Alberta Science and Research Investment Program (ASRIP), and Alberta Synchrotron Institute (ASI) for providing financial support. F.J. is recipient of NSERC University Faculty Award (UFA).

Supporting Information Available: Details for crystal structure of **2** (interatomic distances and atomic coordinates), electronic absorption spectroscopy, Raman spectroscopy (spectra of the oxidized solutions; curve-fitting of the Mo═O peak; Raman band assignments for solids **1**−**3**; DFT calculations of Raman spectra), Mo K-edge XAS (comparison between EXAFS spectra of Mo(V) in 7.4−9.4 M and 1.7−2.7 M HCl with those of **1**−**3**), PCA analysis of the EXAFS spectra, EXAFS simulation of Mo_2O_3 species, Mo $L_{2,3}$-edge XANES spectra, and ADF calculations of the molecular orbitals (Appendices 1−9). This material is available free of charge via the Internet at http://pubs.acs.org.

IC062047C